

An experimental study of hull girder loads on an intact and damaged naval ship

E. Begovic^{a,*}, A.H. Day^b, A. Incecik^b

^a Department of Industrial Engineering, University of Naples Federico II, Via Claudio 21, Naples, Italy

^b Department of Naval Architecture Ocean and Marine Engineering, University of Strathclyde, Glasgow, UK

ARTICLE INFO

Keywords:

Experimental shear force and bending moments assessment
Roll decay
Equivalent linear roll extinction coefficient

ABSTRACT

The study reported in this paper is focused on experimental investigation of the hull girder loads on an intact and damaged naval ship DTMB 5415 at zero speed. The experimental campaign was carried out in head and beam regular waves at the University of Strathclyde. The effect of the use of moorings in the model experimental setup was investigated in the context of loads assessment, and the moorings are shown to influence the measured hull girder loads at some wave frequencies compared to the free drift case. Therefore the tests in beam seas are performed with free drifting model while the moored model setup was adopted for head seas. The results for ship motions are compared with those from a previous campaign giving an insight into repeatability and uncertainty of measurements. The roll decay of the ship in both intact and damaged conditions is analysed and the linear and quadratic extinction coefficients for the model and the ship scale are reported and detailed discussion on intact-versus-damaged ship roll damping behaviour is given. The results for the hull girder loads are presented for intact and damaged ship. An investigation of the nonlinear effects due to wave height variation in the range wave height to wave length from 1/50 to 1/22 on the shear force and bending moment values was carried out for a range of wave lengths to ship length ratios from 0.8 to 1.4. The results of the extensive campaign are compared against similar experimental studies forming a benchmark data for validation of numerical methods.

1. Introduction

The determination of the hydrodynamic loads and the evaluation of structural responses are key elements in a sound design procedure for ships and offshore structures. A growing interest in accurate prediction of hydrodynamic loads was highlighted by Hirdaris et al. (2014) who reported that approximately 47% of papers published in the period from 2008 to 2012 in international peer-reviewed journals are dedicated to research and development activities related to the computation of wave-induced loads, followed by specialist ship structure topics (slamming, sloshing, etc.), fatigue loads and uncertainties in wave load modelling and validation. Although wave load prediction can be implemented at a wide range of levels of complexity, starting from simple potential strip theory up to fully nonlinear methods (e.g. RANS CFD simulations), the authors pointed out that the numerous partly nonlinear or blended methods require verification against experimental data. Furthermore they highlighted the necessity for quality benchmark data, particularly for measurements of global hull girder loads from model tests.

A variety of experimental results (Fonseca and Guades Soares, 2002) has demonstrated that the wave induced vertical bending moments (VBM) shows a nonlinear behaviour for ships with small block coefficients, such as container ships, naval ships, frigates and destroyers, and some passenger ships. The nonlinearities of vertical bending moment relate to three different aspects: the asymmetry of the peaks in the time series, a non-linear variation of the transfer function with the wave amplitude, and higher order harmonics of the time signals.

Among the first studies dealing with experimental data on the vertical responses of ship models in regular and irregular waves with an emphasis on the nonlinear effects are Watanabe et al. (1989) and O'Dea et al. (1992). Both authors tested the S-175 ITTC benchmark container ship, reporting for the first time second order harmonics of VBMs and systematic variation of the first harmonic and phase angle with the wave steepness.

Fonseca and Guades Soares (2002) presented a partly-nonlinear time domain method, accounting for nonlinear hydrostatic restoring and calculating Froude-Krylov forces on the instantaneous wetted

* Corresponding author.

E-mail address: begovic@unina.it (E. Begovic).

Nomenclature

A	wave amplitude, m	TM	torsional moment, N m
B_{OA}	beam over all, m	V	displacement volume, m ³
B_{WL}	beam at waterline, m	VBM	vertical bending moment, N m
C_B	block coefficient	VSF	vertical shear force, N
C_M	midship section coefficient	Δ	displacement, kg, tons for ship scale
C_P	prismatic coefficient	φ	roll angle, rad
D	depth, m	η _{3/A}	non-dimensional heave response
g	acceleration of gravity, 9.80665 m/s ²	η _{4/kA}	non-dimensional roll response
GM	transversal metacentric height, m	η _{5/kA}	non-dimensional pitch response
H	wave height, m	η _i	measured motion, i=3, 4, 5 corresponds to heave, roll and pitch respectively
HBM	horizontal bending moment, N m	λ	ship model scale factor
HSF	horizontal shear force, N	λ _w	wave length, m
H/λ_w	ratio between wave height and wave length	λ _{w/LOA}	wave length to ship length ratio
k	wave number, $2\pi/\lambda_w$	ρ	water density, kg/m ³
KG	vertical position of the centre of gravity, from BL, m	ω _{E(LPP/g)} ^{0.5}	non-dimensional encounter wave frequency
KM	vertical position of the metacentre, from BL, m	ω	wave frequency, rad/s
k_{XX}	radius of gyration with respect to x axis, m, $k_{XX} = \sqrt{\frac{I_{XX}}{A}}$	ω _E	encounter wave frequency, rad/s
k_{YY}	radius of gyration with respect to y axis, m, $k_{YY} = \sqrt{\frac{I_{YY}}{A}}$	ω _{ϕ0}	roll natural circular frequency, rad/s
k_{ZZ}	radius of gyration with respect to z axis, m, $k_{ZZ} = \sqrt{\frac{I_{ZZ}}{A}}$	ω _ϕ	roll damped circular frequency, rad/s $\omega_\phi = \sqrt{\omega_{\phi0}^2 - \alpha_{eq}^2}$
LCG	longitudinal position of the centre of gravity from transom, m	α	linear extinction coefficient, 1/s, $\alpha = \frac{B_1}{2l_\phi}$
LOA	length over all, m	α _{eq}	equivalent linear extinction coefficient, $\alpha_{eq} = 2\alpha + \frac{4}{3\pi}\omega_\phi\phi\beta + \frac{3}{8}\omega_\phi^2\phi_a^2\gamma$
L_{PP}	length between perpendiculars, m	β	quadratic extinction coefficient, 1/rad, $\beta = \frac{B_2}{l_\phi}$
T	draught, m	γ	cubic extinction coefficient, 1/rad ² , $\gamma = \frac{B_3}{l_\phi}$
T_ϕ	natural roll period, s	ϕ _{MEAN}	mean roll angle, rad, $\phi_{MEAN} = \frac{ \phi_1 + \phi_{t+1} }{2}$
T_W	incident wave period, s		

surface of the ship. The numerical method was verified with the experimental results of Watanabe and O'Dea, showing that the method is able to capture the nonlinearities in vertical motions, accelerations and vertical bending moment values. Important experimental studies on the assessment of vertical loads acting on the ITTC S-175 container ship in regular and irregular waves were presented by Fonseca and Guades Soares (2004a, 2004b). Tests in regular waves were performed over a range of non-dimensional wave frequencies, with waves varying from $\lambda/L_{PP}=0.5$ –3. For each wave frequency several wave amplitudes were used ranging from small to large amplitude and thus the influence of the wave amplitude on the nonlinear characteristics of the responses was assessed. The measured responses include the absolute and relative motions, vertical accelerations, and cross-sectional loads at midship and 1/4 L_{PP} from the forward perpendicular. Irregular wave tests were carried out for three sea states; the reported probability distributions of the positive and negative peaks of motions and loads, indicated that the Rayleigh distribution cannot be used for wave-induced vertical loads.

Song et al. (2011) presented a weakly nonlinear 3D time domain Rankine panel method validation on a 6500 TEU container ship segmented model in small and large wave amplitudes over a wide range of wave frequencies. Results were presented as first-order response amplitude operators (RAOs) and time histories; second order harmonics were not reported. The authors reported that the nonlinear effects were observed for the three highest waves (wave heights of 5, 7 and 10 m in ship scale). They concluded that the weakly-nonlinear method developed shows a very good overall agreement with the experimental data, and in particular better agreement for vertical than for horizontal and torsional loads for moderate wave heights, and acceptable to poor agreement at the steepest wave.

Kukkanen and Matusiak (2014) presented a nonlinear time domain calculation method based on Green's functions to predict the RoPax hull girder loads. Model test results of ship motions, vertical shear forces and bending moments at two sections at zero speed and Fr=0.25

were given for calm water, regular and irregular head waves. The results were presented for the first order RAO and phases for motions and loads. The results obtained from the numerical method are in good agreement with the reported experimental data, although authors did not comment on the ability of the numerical method to predict the effect of wave height variation.

Zhu and Moan, (2013, 2014) presented extensive model tests on ultra-large containerships of 8600-TEU and 13000-TEU conducted in head seas in regular and irregular waves with focus on the nonlinear vertical responses in severe seas. The authors reported that in irregular waves, the motion peaks and troughs generally follow a Rayleigh distribution and that the asymmetries between positive and negative peaks are limited and less pronounced than expected from existing empirical formulas or state of the art tools.

It should be noted that the majority of works on structural responses have addressed intact ship loads; however in the last decade some investigations on loads in damaged conditions have been presented. Korkut et al. (2004) presented experimental results for motions of an intact and damaged RoRo ship in regular waves at zero speed. The effects of wave amplitude variation in head, beam and quartering seas were investigated. In Korkut et al. (2005) experimental results for the global loads on an intact and damaged Ro-Ro ship model in regular waves are presented. The very extensive experimental campaign comprises nine frequencies in head, beam and stern quartering seas varied over four wave heights. The conclusions highlight the main experimental findings illustrating the effect of damage on the loads; in general the structural response of the damaged model are greater than those for the intact ship for most of the headings with the exception of the horizontal bending moments in beam seas. The results also show the variation of the load responses with the wave amplitude depending on the wave frequency.

Lee et al. (2012) developed a computational tool based on a two-dimensional linear method to predict the hydrodynamic loads on damaged ships. The results of the theoretical method and an experi-

Table 1

Main particulars of Notional US Navy Destroyer Hull 5415.

Particulars	Ship	Model 51
L _{OA} (m)	153.300	3.0
L _{PP} (m)	142.200	2.788
B _{WL} (m)	19.082	0.374
B _{OA} (m)	20.540	0.403
D (m)	12.470	0.244
T (m)	6.150	0.120
V (m ³)	8424.4	0.0635
Δ (t, kg)	8635	63.5
C _B	0.505	0.505
C _P	0.616	0.616
C _M	0.815	0.815
KM (m)	9.493	0.186
KG (m)	7.555	0.148
GM (m)	1.938	0.038
LCG (m)	70.137	1.375
k _{xx} -WATER (m)	6.932	0.136
k _{yy} -AIR (m)	36.802	0.696
k _{zz} -AIR (m)	36.802	0.696

**Fig. 1.** DTMB 5415 model, positions of bulkheads and load cell.**Table 2**

Position of watertight bulkheads.

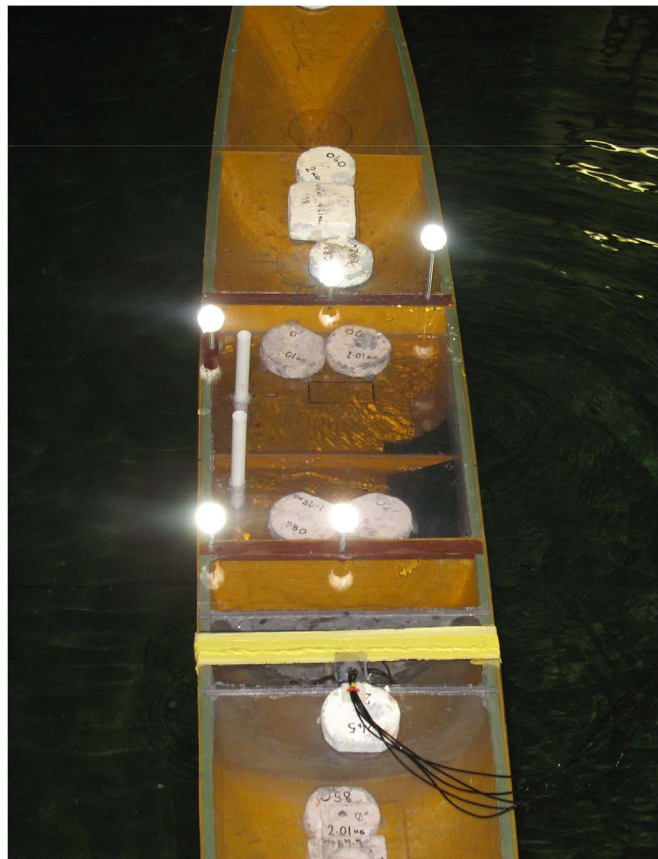
Compartment	Distance from AP	
	x ₁ (m)	x ₂ (m)
Aft_peak	0	30.86
Comp_2	30.86	65.66
Comp_3	65.66	76.15
Comp_4	76.15	90.02
Comp_5	90.02	108.63
Comp_6	108.63	130.56
Forward_Peak	130.56	142.20

mental campaign on a 1/100 scale model of the well-known DTMB 5415 frigate hull tests were compared over a variety of design conditions. The comparison demonstrated fair prediction of vertical and horizontal bending moments and poor accuracy for torsional moment predictions.

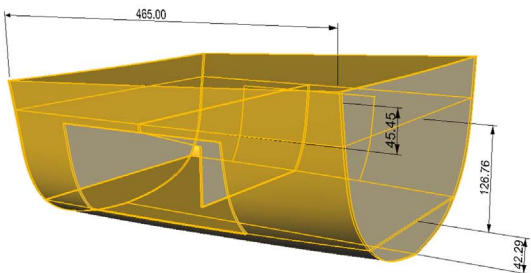
Begovic et al. (2011) presented results obtained from an experimental test program at the University of Strathclyde in which the ship model used was the same as in the study reported in Lee et al. (2012). In addition to the model tests, the motion RAOs for the intact and damaged ship model were compared with calculations using MARINTEK's ShipX -2D time domain software[®] code, showing fairly good agreement for global load predictions. In Begovic et al. (2013), the motion response characteristics of the DTMB Model 5415 in intact and damaged conditions in head, beam and quartering seas at zero speed were presented based on measurements carried out with a 1:51 scale model. Experimental results were presented as the first and second harmonics of the RAOs of heave, roll and pitch. A detailed discussion on intact-versus-damaged ship behaviour is given, taking into considerations the influence of the flow interaction between the

ship, the environment and the orientation of the opening. Furthermore the effect of model scale is discussed according to the results of two test campaigns carried out at different scales. Domeh et al. (2015) presented an experimental study on segmented Leander class frigate model in waves at zero and forward speeds. The novelty of the experimental campaign was systematic permeability and damage orifice size variations' influence on the vertical motions of damaged hull. In Parunov et al. (2015) the case study to determine the vertical motions and hull girder bending moments of damaged 5415 ship, presented by Lee et al. (2012) is presented. Authors compared the results from commonly used the added mass method and the lost buoyancy method against the experimental results, reporting that the lost buoyancy method underestimates while the added mass overestimates the experimental vertical bending moments in the whole frequency range.

The present study was focused on the measurement of hull girder loads on a segmented model of the naval benchmark hull DTMB 5415 at zero speed in intact and damaged conditions with particular emphasis on nonlinear effects due to the wave height variation. The experimental campaign, carried out at the University of Strathclyde, consists of motions and loads in head sea for the constant H/λ_w ratio=1/50. An investigation of the nonlinear effects due to the wave height variation on the shear force and bending moment values is carried out for a range of wave lengths to ship length ratios λ_w/L_{OA} from 0.8 to 1.4 for the intact and damaged ship. The tests in beam seas have been carried out both for a soft-moored and a free drifting model, to examine the influence of elastic mooring on loads. The experimental results of heave, roll and pitch motions are presented together with the results of the previous campaign to highlight the repeatability and uncertainty of the measured RAOs. The results for the hull girder loads are presented as non-dimensional vertical shear force, hogging and sagging moments for intact and damaged ship. Furthermore the roll decay tests have been carried out by varying the initial heel angle from 5 degrees to 25 degrees. Detailed discussion on intact-versus-damaged



a. Detail – damage compartment



b. Detail – damage compartment dimensions – model scale (mm)

Fig. 2. a. Detail – damage compartment. b. Detail – damage compartment dimensions – model scale (mm).

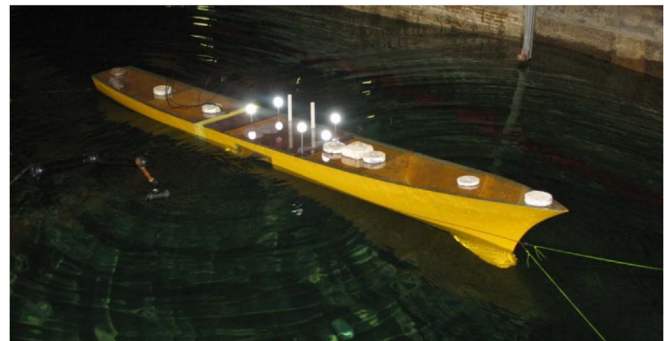


Fig. 3. Experimental setup.

ship roll damping behaviour is given based on the analysis of roll decay.

2. Experimental program

2.1. Description of the facility and equipment

The experiments have been carried out in the Kelvin Hydrodynamic Laboratory at the University of Strathclyde, Glasgow using a 1/51 scale model of the DTMB naval ship 5415. The towing tank is 76 m long, 4.6 m wide and has a water depth of 2.15 m; it is equipped with a multi-flap type absorbing wave maker.

A detailed description of the model is given in Begovic et al. (2013). The main particulars of the DTMB 5415 model are given in Table 1. The model has been fitted with five watertight bulkheads located as shown in Fig. 1 with longitudinal position as reported in Table 2.

The damage opening shown in Fig. 1 leads to two compartment (3 and 4) symmetric flooding. The flooded length extending from $x_1=65.66$ m (ship scale) to $x_2=90.02$ m corresponds to 17% of length between perpendiculars. This extent seems reasonable for a destroyer type ship, as expected this type of ship should maintain all functionality with two compartments damaged. Both compartments were fitted with a small tube to provide an air vent during tests; this is visible on the port side of the model as shown in Fig. 2a. The exact amount of floodwater is determined from hydrostatic calculations: i.e. for the measured immersion and trim angle, the displaced volume was found.

The model is split into two parts at a location corresponding to 55.59 m from the stern at full scale, and joined with a five-component load cell. The watertight integrity of the model is maintained by sealing the joint with a strip of very thin latex, which is sufficiently flexible to transmit no significant shear forces or moments.

The characteristics of the damaged ship are given in Table 3.

2.2. Description of test conditions

The motion and loads characteristics of the model in intact and damaged conditions were investigated in regular waves with zero

Table 3

Two compartments damaged load condition – ship dimensions.

Particulars	Ship
$L_{\text{flooded compartments}}$ (m)	24.360
$x_{1-\text{flooded compartments}}$ (m)	65.66
$x_{2-\text{flooded compartments}}$ (m)	90.02
B_{WL} (m)	19.458
T_{mean} (m)	7.410
Trim [+aft] (degrees)	-0.656
Δ (t)	11273.8
Mass of flooded water (t)	2638.9
LCG (m)	71.622

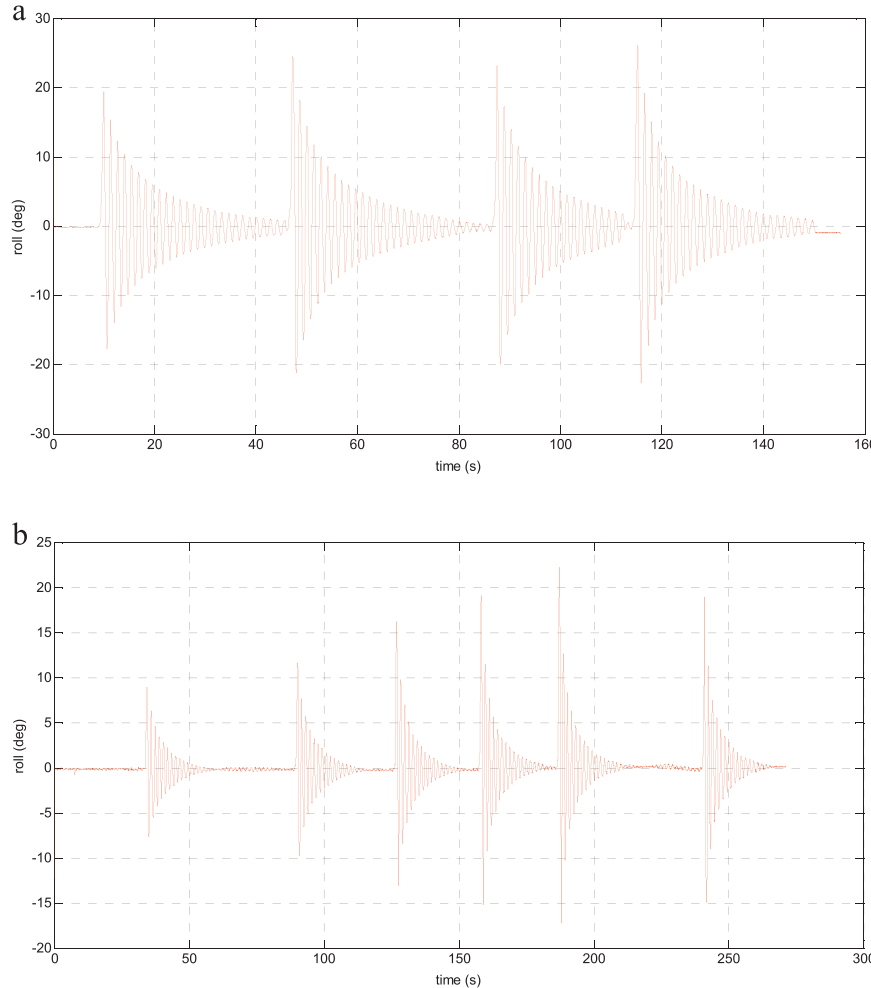


Fig. 4. a. Roll decays of intact model. b. Roll decays of damaged model.

forward speed in both head and beam seas. During the tests, the motion responses of the model in six degrees of freedom were measured using a QUALISYS motion capture system. Five infra-red reflectors were strategically placed on the vessel as shown in Fig. 3. The coordinates of the markers in three dimensional space were measured by four cameras suitably positioned on the towing carriage near the vessel; the six-degree-of-freedom motions are calculated and output in real time. The wave elevation was monitored and recorded using two ultrasonic wave probes, one close to the model and another one close to wavemaker. Loads were measured by a load cell DHI model 206/5C 130. The sampling frequency was 137.36 Hz.

2.3. Roll decay data

To determine the damping coefficients of the intact and damaged ship model, a roll decay tests were carried out in which the roll motion is induced by applying a transverse heel angle and then releasing the model to freely oscillate. The initial heel of the model is induced manually and the inclination angle and subsequent roll motions are measured in real time using the motion capture system. The initial inclination angles varied from 5° to 25° in order to obtain sufficient data to determine both the linear and nonlinear extinction coefficients. Examples of roll decay time histories are given in Fig. 4a and b for the intact and damaged ship respectively. It can clearly be observed from the number of oscillations required to damp the motion to the undisturbed state that the damping of the damaged ship is significantly higher than that of the intact vessel due to the flood water kinematics.

The flood water dynamics acts in a manner similar to sloshing in a

tank filled with the liquid and for the proper determination of its effect on total damping, the kinematics of the flooded water should be considered. In the present study a simple analysis is performed to “quantify” the difference in roll damping of intact and damaged ship following the procedure proposed by Chakrabarti (1994) and Bulian et al. (2009). The one-degree of freedom equation for unforced roll motion is written in the form:

$$(I_{44} + A_{44})\ddot{\phi} + B_{44-\text{total}}(\dot{\phi}) + C_{44}\phi = 0 \quad (1)$$

where I_{44} and A_{44} are the moment of inertia and added moment of inertia respectively, C_{44} is the roll restoring coefficient, $B_{44-\text{total}}$ stands for the nonlinear damping coefficient including viscous effects and ϕ is the roll angle.

The nonlinear damping coefficient $B_{44-\text{total}}$ can be expressed as a series expansion of ϕ and $|\dot{\phi}|$ in the form:

$$B_{44-\text{total}} = B_{44-1}\dot{\phi} + B_{44-2}\cdot\dot{\phi}\cdot|\dot{\phi}| + B_{44-3}\cdot\dot{\phi}^3 \quad (2)$$

Using the ITTC – Recommended Procedures and Guidelines 7.5-02-07-04.5 (2011) nomenclature, Eq. (1) can be rewritten in a more common form as:

$$\ddot{\phi} + 2\alpha\cdot\dot{\phi} + \beta\cdot\dot{\phi}\cdot|\dot{\phi}| + \gamma\cdot\dot{\phi}^3 + \omega_\phi^2\cdot\phi = 0 \quad (3)$$

where

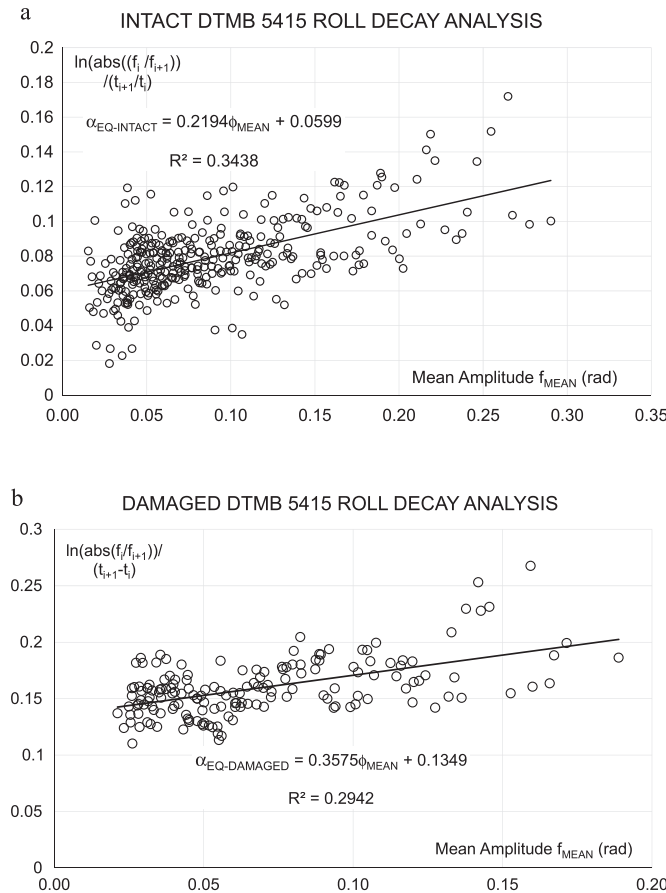


Fig. 5. a. Roll decay coefficients analysis – Intact model. b. Roll decay coefficients analysis – Damaged model.

Table 4

Roll natural period and frequency and extinction coefficients.

	Intact ship		Damaged ship	
	Model	Ship	Model	Ship
T _φ (s)	1.3699	9.7832	1.5249	10.8902
ω _{φ0} (rad/s)	4.5873	0.6423	4.1235	0.5774
ω _φ (rad/s)	4.5866	0.6422	4.1203	0.5770
α (1/s)	0.0599	0.0084	0.1349	0.0189
β (1/rad)	0.1127	0.1127	0.2043	0.2043

$$\begin{aligned} \alpha &= \frac{B_{44-1}}{2(I_{44} + M_{44})} \text{ linear extinction coefficient} \\ \beta &= \frac{B_{44-2}}{I_{44} + M_{44}} \text{ quadratic extinction coefficient} \\ \gamma &= \frac{B_{44-3}}{I_{44} + M_{44}} \text{ cubic extinction coefficient} \\ \omega_{\phi 0} &= \sqrt{\frac{C_{44}}{I_{44} + M_{44}}} = \frac{2\pi}{T_{\phi}} \text{ natural roll frequency} \end{aligned} \quad (4)$$

Furthermore, using Fourier expansions for the non linear term:

$$\dot{\phi} \cdot |\phi| \approx \frac{8}{3\pi} \cdot \omega_{\phi} \cdot \phi_i \cdot \dot{\phi} \quad (5)$$

where ϕ_i is the amplitude of the i -th oscillation cycle and ω_{ϕ} is the frequency of oscillation in the i -th cycle

it is possible to reformulate Eq. (3) in linearized roll equation as:

$$\ddot{\phi} + 2\alpha_{eq}\dot{\phi} + \omega_{\phi}^2 \cdot \phi = 0 \quad (6)$$

Where the equivalent linear extinction coefficient is defined as:

$$\alpha_{eq} = \alpha + \frac{4}{3\pi} \cdot \omega_{\phi} \cdot \phi_i \cdot \beta + \frac{3}{8} \cdot \omega_{\phi}^2 \cdot \phi_i^2 \cdot \gamma = \frac{B_{44-total}}{2(I_{44} + A_{44})} \quad (7)$$

Although in **ITTC Recommended Procedures and Guidelines 7.5-02-07-04.5 (2011)**, the decrement of decay curve is given by $\Delta\phi = |\phi_i| - |\phi_{i+1}|$, in this work logarithmic decay has been applied according to [Chakrabarti \(1994\)](#) and [Bulian et al. \(2009\)](#).

$$\begin{aligned} \Delta\phi &= \ln\left(\frac{|\phi_i|}{|\phi_{i+1}|}\right) \text{ under the condition that } \Delta\phi \rightarrow 0 \text{ and} \\ \alpha_{eq,i-log} &\approx \frac{1}{t_{i+1} - t_i} \ln\left(\frac{|\phi_i|}{|\phi_{i+1}|}\right) \equiv \alpha + \frac{4}{3\pi} \cdot \omega_{\phi} \cdot \phi_{MEAN-i} \cdot \beta \end{aligned} \quad (8)$$

Where ϕ_{MEAN} is defined by:

$$\phi_{MEAN} = \frac{|\phi_i| + |\phi_{i+1}|}{2} \quad (9)$$

and natural roll frequency:

$$\omega_{\phi 0} = \sqrt{\omega_{\phi}^2 + \alpha_{eq}^2}$$

For both intact and damaged ship, about 10 decay tests have been carried out. From the recorded roll motions, the first cycle has been removed and the next 16 cycles for intact and 7 for damaged ship, have been analysed. The calculated equivalent roll extinction coefficient for the intact and damaged ships α_{EQ} as a function of the mean amplitude are given in Fig. 5a and b. From the trend lines shown as in the form $\alpha_{EQ}=ax+b$, the extinction coefficients are calculated as:

$$\begin{aligned} \alpha &\equiv b \\ \beta &\equiv \frac{3\pi}{4 \cdot \omega_{\phi}} \cdot a \end{aligned}$$

To scale up the model values to the ship scale, the following relations are valid:

$$T_{\phi-SHIP} = T_{\phi-MODEL} \cdot \sqrt{\lambda}$$

$$\omega_{\phi-SHIP} = \frac{\omega_{\phi-MODEL}}{\sqrt{\lambda}}$$

$$\alpha_{SHIP} = \frac{\alpha_{MODEL}}{\sqrt{\lambda}}$$

$$\beta_{SHIP} = \beta_{MODEL}$$

The results of the roll decay experiments: natural period of roll, natural roll frequency, damped roll frequency, linear and quadratic extinction coefficients for the intact and damaged ship are given in Table 4.

Table 4 shows that the damaged ship exhibits higher roll natural period as well as much higher linear and quadratic extinction coefficients α and β . As stated before, this difference is mainly due to the flood water dynamics inside and outside the compartment, generating some waves and some vortices. It can be noted that both extinction coefficients have doubled. Similar results on the roll damping behaviour have been reported by [Manderbacka et al. \(2015\)](#) who studied experimentally coupling of the flooded water and ship motions for the box shaped barge model. Authors reported that the evaluated damping ratio is three to six times higher than for the intact ship depending on the compartment geometry and amount of flooded water. It has to be highlighted that this comparison should not be considered as quantitative comparison, but only as the trend of data; the fair quantitative comparison of damping characteristics is impossible due to differences in experimental setup (in Manderbacka the focus was on sloshing inside and the compartment was closed once filled with water) and in the presentation of the results (damping ratio versus extinction coefficients).

In order to examine how well this simplified damping model reflects the behaviour, the time histories of the roll decay were reconstructed using the values obtained above via a Runge-Kutta simulation for both intact and damaged cases, for decay cases with an initial angle of

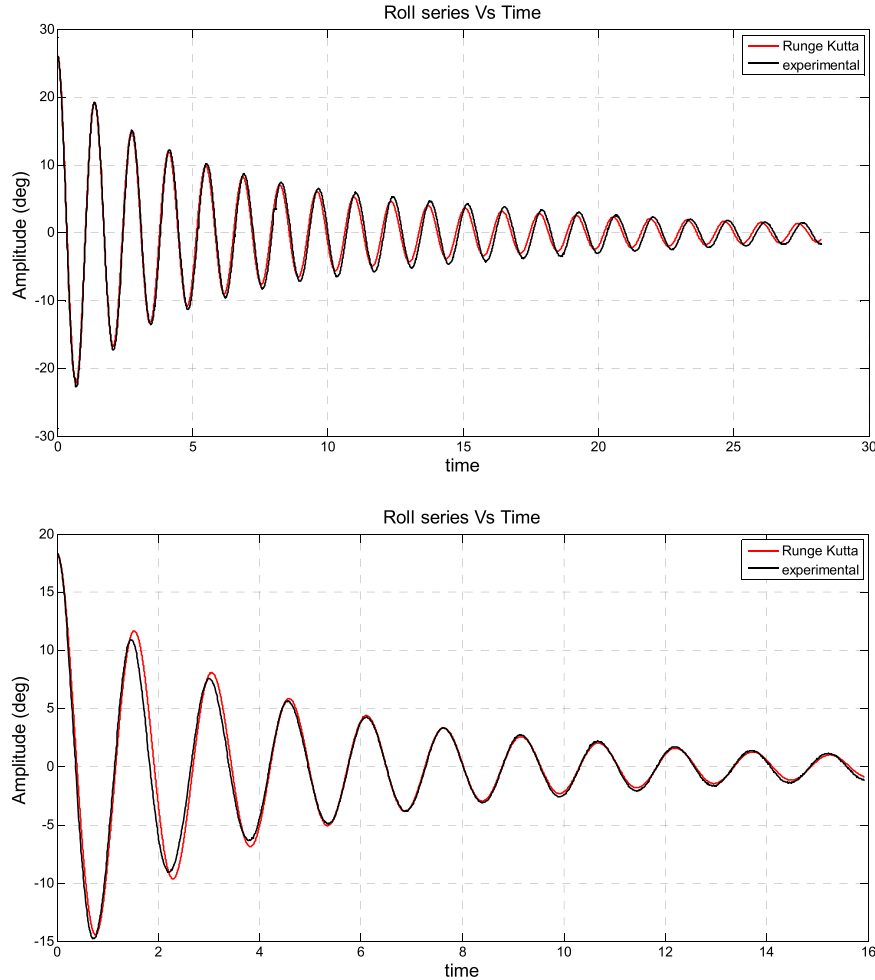


Fig. 6. Prediction of roll decay by equivalent roll damping coefficients for intact (upper) and damaged (lower) model.



Fig. 7. Roll motion of intact and damaged ship.

approximately 20 degrees. These results are shown in Fig. 6. It can be seen that although the damping model is not perfect, the extinction coefficients, reported in Table 4, predict the global trend well and can be used in more complicated simulations of damaged ship behaviour.

To illustrate how the flooding affects the roll motion responses, the results for the roll motion of the intact and damaged ship are shown in Fig. 7. It can be seen that the roll of the damaged ship is clearly lower at frequencies less than the resonance frequency. At the roll resonance frequency the intact ship has a value of roll RAO of 7.2 against a

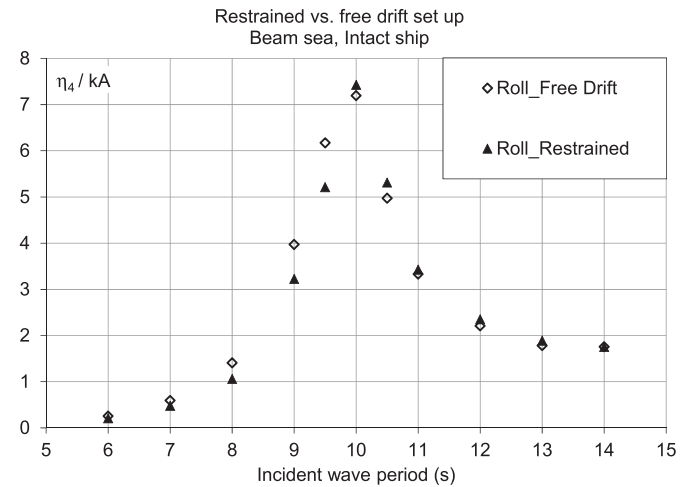


Fig. 8. Non-dimensional roll motion.

corresponding value for the damaged ship of 4.76. At waves with periods higher than 11 s, the damaged ship has higher response values.

2.4. Restrained vs. free drift test setup

In the stationary tests models were moored to the tank walls as shown in Fig. 3. Soft elastic restraints were placed as close to the waterplane as possible and were always very slack. The measured natural frequency of the restraint, evaluated from free oscillations tests

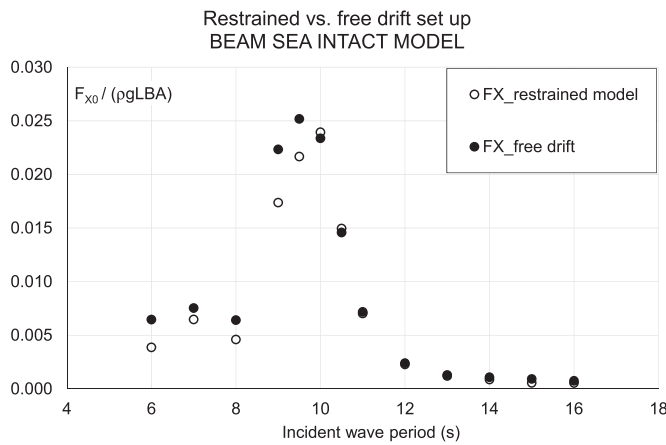


Fig. 9. Non-dimensional horizontal shear force.

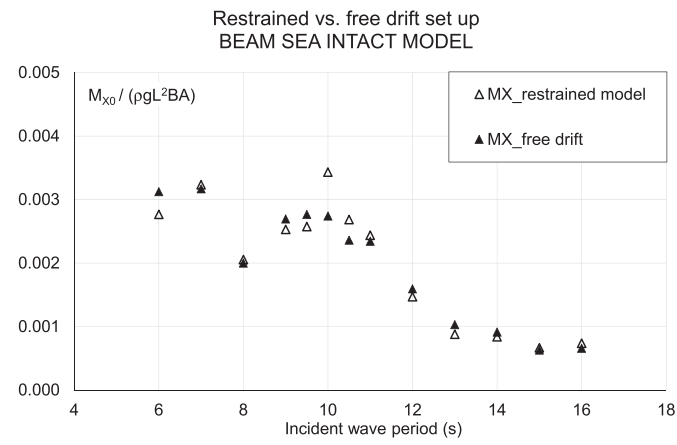


Fig. 12. Non-dimensional vertical bending moment.

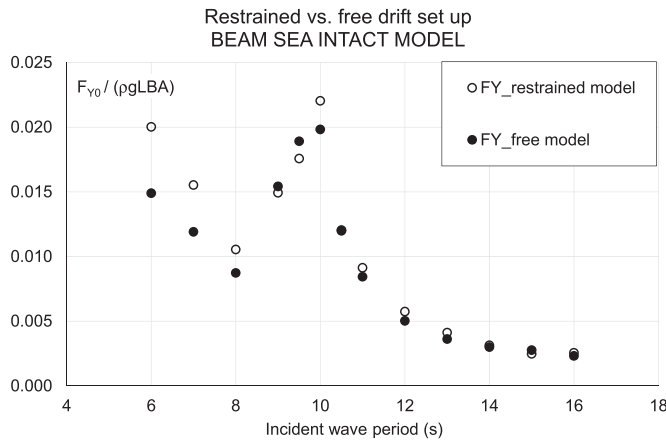


Fig. 10. Non-dimensional vertical shear force.

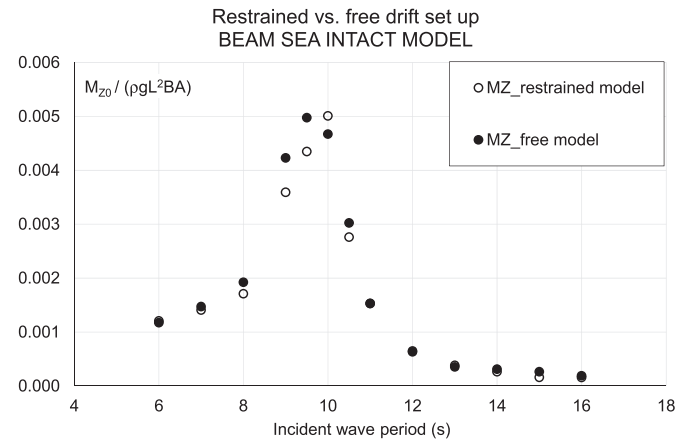


Fig. 13. Non-dimensional torsional moment.

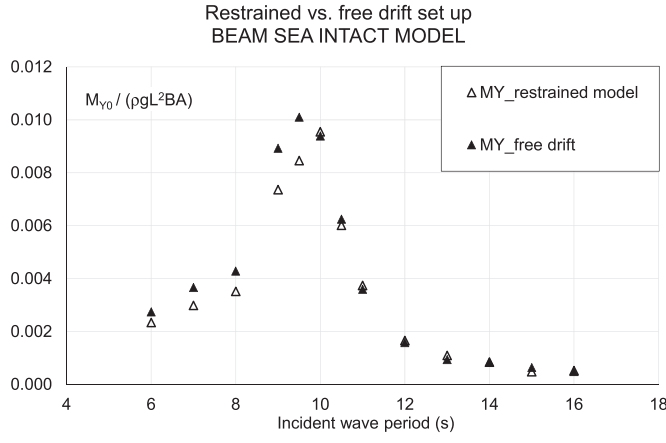


Fig. 11. Non-dimensional horizontal bending moment.

investigated by performing the tests for the intact ship in both restrained and free drifting conditions in beam seas.

The results of these tests are given in Figs. 8–13 showing the roll motion, horizontal and vertical shear forces, horizontal and vertical bending moments and torsional moment, respectively. The wave steepness ratio H/L_W was held constant for these tests at 1/50. It can be seen from Fig. 8 that for the roll motions there is relatively little difference between the two experimental setups except at the wave periods corresponding to 9 and 9.5 s, as experienced in the previous experimental campaign. However it can be seen from Figs. 9, 11 and 13 that the resonance peaks in the measured horizontal shear forces (HSF), horizontal bending moments (HBM) and torsional moments (TM) shift somewhat. This cannot be explained by the change in encounter frequency resulting from the drift velocity, which was generally extremely small (velocity of model has an order of magnitude 2 cm/s). It can be seen from all measured loads that there is no difference for the wave periods higher than 10 s but there are some differences within 10% at the wave periods of 9 and 10 s. As a result of these tests for the beam seas the free drift setup was chosen while the moored model setup was adopted for head seas. A complete summary of tests carried out is given in Table 5.

3. Results of motion measurements – repeatability and uncertainty analysis

This campaign was focused primarily on the loads measurements during the tests in the same conditions as reported in Begovic et al. (2013), i.e. for wave periods from 6 to 14 s, covering a range of wave length over ship length ratio from 0.4 to 2.0. The repeatability of the motion measurements as part of the uncertainty assessment is

in surge, was found to be 0.03 Hz, which is an order of magnitude less than any wave frequency considered, as recommended by the ITTC (Recommended Procedures and Guidelines 7.5-02 07–03.1).

In the previous experimental campaign (Begovic et al., 2013) it was found that the restraint system did not significantly influence the motion responses and thus all tests were carried out with a soft-restrained model. In the present test campaign, the effect of the restraint system on the shear force and bending moment values was

Table 5
Test matrix – Model 51.

Test ID	Heading	Condition	T _W (s)	H/λ	Figure	
Setup settling	Free-Restrained	Beam sea	Intact	6–14	1/50	8–13
Heave, Pitch	Restrained	Head sea	Intact	6–14	1/50	14,15
Roll	Free drift	Beam sea	Intact	6–14	1/50	16
Heave, Pitch	Restrained	Head sea	Damaged	6–14	1/50	17,18
Roll	Free drift	Beam sea	Damaged	6–14	1/50	19
Time history	Restrained	Head sea	Intact	10	1/50	20a, 20b
VSF, HOG, SAG	Restrained	Head sea	Int-Dam	6–14	1/50	21–23
Global loads	Free drift	Beam sea	Int-Dam	6–14	1/50	24–28
Time history	Restrained	Head sea	Intact	10	Varied	29–31
VSF, VBM	Restrained	Head sea	Int-Dam	9,10,11,12	Varied	32–35
Global loads	Free drift	Beam sea	Intact	10	Varied	36, 37

INTACT SHIP - HEAD SEA

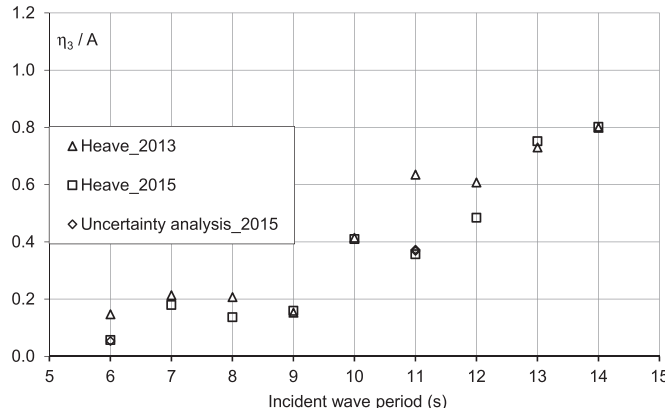


Fig. 14. Repeatability of heave.

INTACT SHIP - BEAM SEA

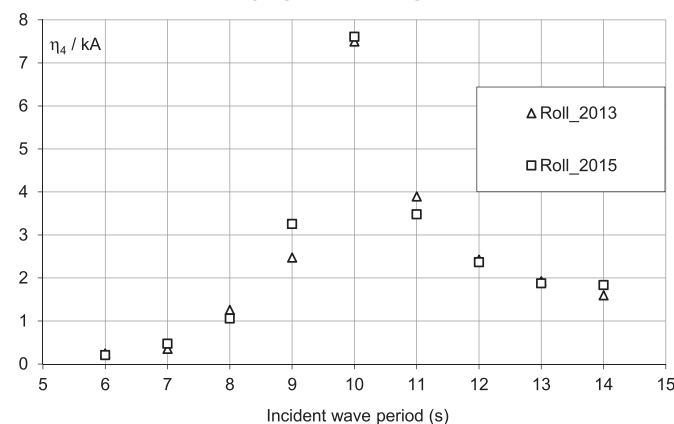


Fig. 16. Repeatability of roll – free drift set up.

INTACT SHIP - HEAD SEA

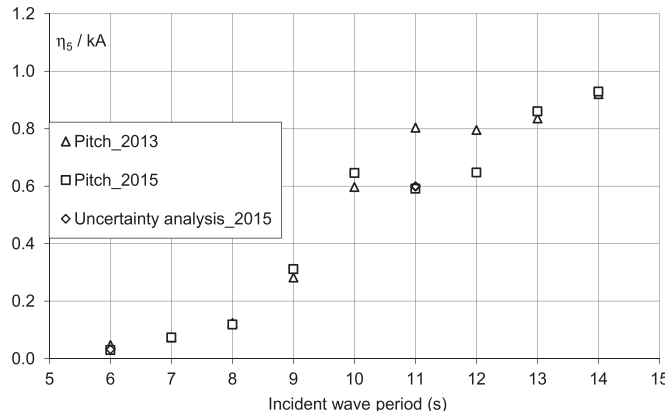


Fig. 15. Repeatability of pitch.

controlled for the intact and damaged ship motions and all the results are given in Figs. 14–19.

The repeatability analysis started from the re-ballasting of the model, the re-setting of the centre of gravity position and the radii of gyration and the mooring of the model on the tank walls. After obtaining the same values, the testing campaign started. It can be seen that the heave and pitch motions in head seas, shown in Figs. 14 and 15, are almost identical for the wave periods shorter than 9 s and longer than 11 s. Both responses show strong dependency on amplitude at wave periods from 9 s to 11 s, where the bigger difference among results of the same campaign was observed. This must be regarded as unexplained at present. In same figures the repeated measurements are given for further uncertainty analysis.

Regarding the intact ship roll RAOs, shown in Fig. 16 there is almost no difference for all the waves tested. The results for the

DAMAGED SHIP - HEAD SEA

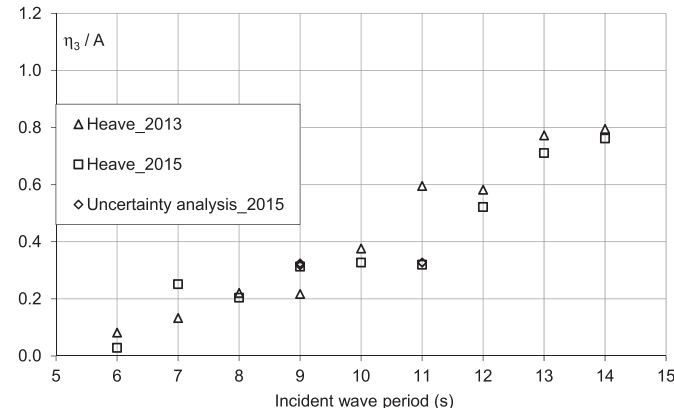


Fig. 17. Repeatability of heave – damaged ship.

damaged ship RAOs for heave, pitch and roll are shown in Figs. 17–19, respectively. Small differences in the heave and pitch RAOs for damaged ship are of the same order as for the intact ship. The damaged roll RAOs, given in Fig. 19 present small differences between two experimental campaigns only for the wave periods higher than 12 s.

The ITTC recommendations 7.5-02-07-02.1 have been followed in the uncertainty analysis to explore the ISO GUM Type A (random) uncertainty and Type B (systematic) uncertainty. Some of the tests were repeated (indicated in diagrams by UA_2015) and to standard deviation of the set of repeated tests, a confidence factor of 1.96 was applied in order to indicate the 95% confidence level. The results showed that the 95% confidence interval for the heave RAOs related to Type A uncertainty lay between 1.5–3% for all cases, both intact and

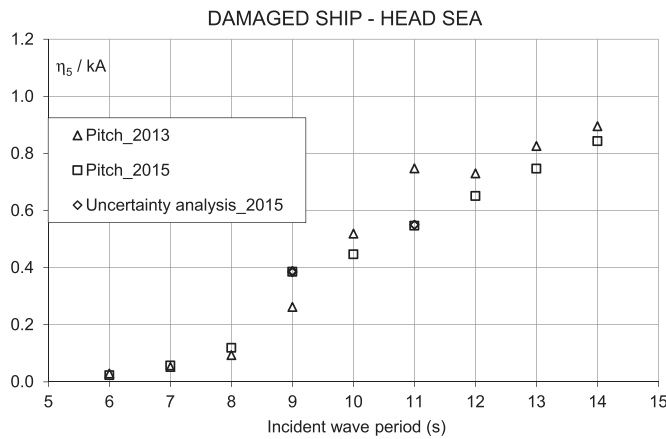


Fig. 18. Repeatability of pitch – damaged ship.

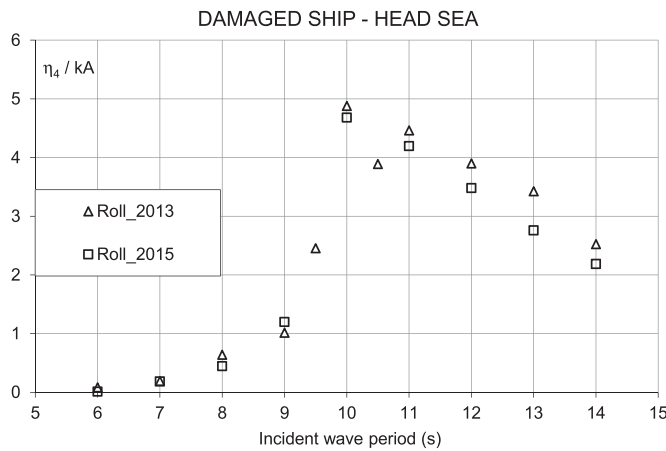


Fig. 19. Repeatability of roll.

damaged. The corresponding interval for the pitch RAOs lay in the region of 3–4%, whilst the confidence interval for the roll RAOs was found to be less than 2% for the intact cases, but typically between 4% and 5% for the damaged cases.

The main components of Type B (systematic) uncertainty are expected to result from the key measurement systems employed: the wave probes and the motion capture system. Day et al. (2011) explored the uncertainty related to calibration of different wave probe systems and estimated the 95% confidence values for the systems adopted in the present study as being between 0.5 and 0.8 mm. The Type B uncertainty related to measurement of model motions using an optical motion capture system can be gained from the body residuals, which are typically substantially less than 0.5 mm.

The other key source of systematic uncertainty results from the load cell, and in particular the uncertainty associated with the calibration. The 5-DOF load cell was calibrated in three stages: first F_y and M_x , secondly F_x and M_y , and finally M_z . In each of the first two cases the load cell was calibrated in 36 steps in both ascending and descending loads. In these cases, the loading was repeated three times, with the lever arm of the load varying between repeats, so that the same set of applied shear forces generated different bending moments. The calibration constants for each of the four components (F_x , F_y , M_x , M_y) were generated using the results from all three repeats. In the case of M_z , only one loading set was applied. The standard error estimate was then calculated using the calibration coefficients determined, and the 95% uncertainty estimated from the standard error using a coverage factor of 2. These uncertainties were expressed as a percentage of the maximum loading applied during calibration. The values obtained for F_x and F_y were 1.1% and 0.9% respectively, whilst the correspond-

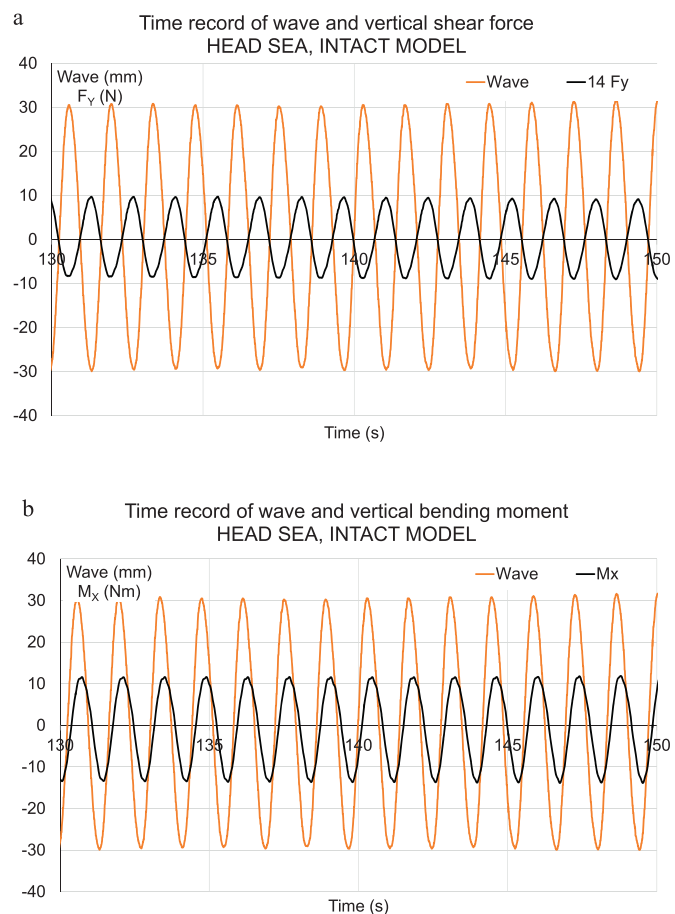


Fig. 20. a. Registration of vertical shear force. b. Registration of vertical bending moment.

ing values for M_x , M_y and M_z were 1.5%, 2.0% and 0.5%.

4. Loads measurements – intact vs damaged ship

The global wave induced loads for intact and damaged ship have been measured at a longitudinal position $x=1.09$ m from the stern, corresponding to the 0.364 L_{OA} , by DHI 206/5C 130 five component load cell. The examples of time series of the measured vertical shear force and vertical bending moment values are given in Fig. 20. The vertical and horizontal shear force amplitudes are calculated as a half of crest-trough distance from the time series. The sag and hog amplitudes were obtained as positive and negative maxima from the zero, after the mean value has been removed from the data. The shear force and bending moment values were divided by $\rho g L_{OA}^2 B_{OA} A$ respectively to obtain the non-dimensional hull girder loads:

$$\begin{aligned} VSF, HSF &= \frac{F_0}{\rho g L_{OA}^2 B_{OA} A}, \\ M_{SAG} &= \frac{M_{0-SAG}}{\rho g L_{OA}^2 B_{OA} A} \\ \text{and } M_{HOG} &= \frac{M_{0-HOG}}{\rho g L_{OA}^2 B_{OA} A} \end{aligned} \quad (10)$$

where A is the wave amplitude.

The vertical shear force (VSF) and vertical bending moment (VBM) values are shown in Figs. 21–23 for the intact and damaged ship in head seas. It can be seen that both the VSF and VBM values are significantly larger for the damaged vessel, with the differences greater in the VSF values than the VBM values.

The loads measurements of intact vs. damaged ship in beam seas, in free drift test set up, are presented for horizontal shear force (HSF)

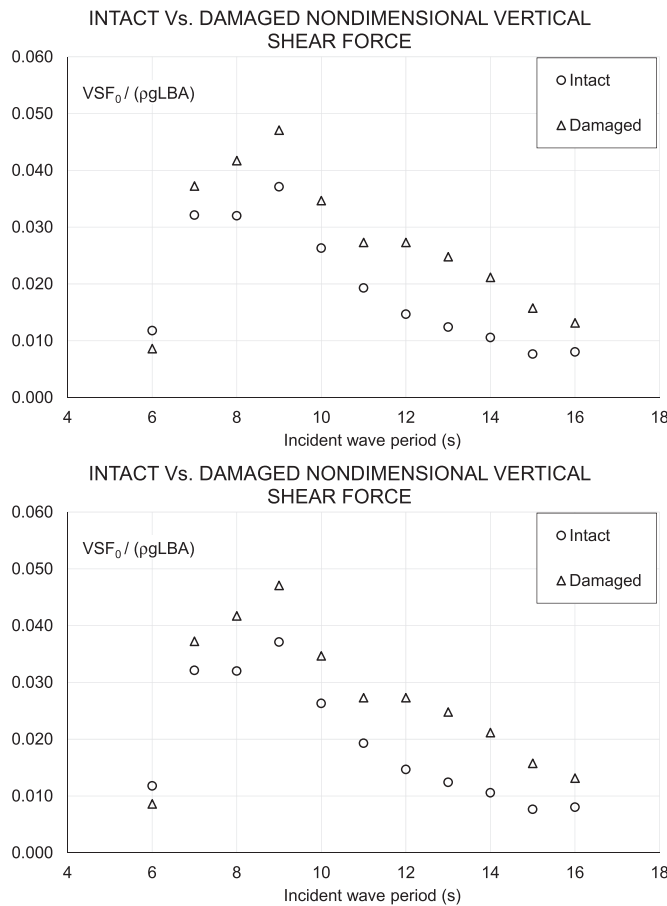


Fig. 21. Non-dimensional vertical shear force- intact vs. damaged ship in head sea.

values and vertical shear force (VSF) values in Figs. 24 and 25. The comparison of moments in beam seas is given only for the positive peaks (SAG definition) of horizontal, vertical and torsional moments and are shown in Figs. 26–28.

It can be noted that the HSFs of the damaged ship are significantly higher than for the intact case in the whole wave range tested, whilst the maximum HSF response is shifted from 9.5 s for the intact ship to 10 s for the damaged ship. It can be noted from Figs. 25–27 that the VSF, HBM and TM values of the intact ship are higher than the corresponding values for the damaged ship, as previously highlighted by Korkut et al. (2005). This behaviour in beam seas is directly related to the lower RAOs of roll motion in this symmetric damage scenario.

Buzanic-Primorac et al. (2015) reported that the ABS and the IACS are applying a factor of increase of still water bending moment SWBM due to the damage equal to 1.10, although some authors in the literature have reported values up to 2.38. Similar results were also observed in this study: for each wave condition tested in head seas, the ratio of the bending moment and the shear force values of the damaged to those of the intact ship is given in the Table 6. The results for the vertical bending moments: sagging and hogging, shown in Table 6, are somewhat higher than the factor used by the ABS and the IACS, but this could be due to the presence of waves. It can be noted that the sagging ratio is higher than the hogging. Regarding the VSF values the ratio is up to 2.06. At the present moment, there are no similar results, available in the literature to compare against.

5. Nonlinear variation of loads with wave amplitude

In the previous tests the steepness ratio H/λ_W was held constant at 1/50. The nonlinearities in loads were investigated for both intact and damaged ship in head and in beam seas. In head seas the amplitude

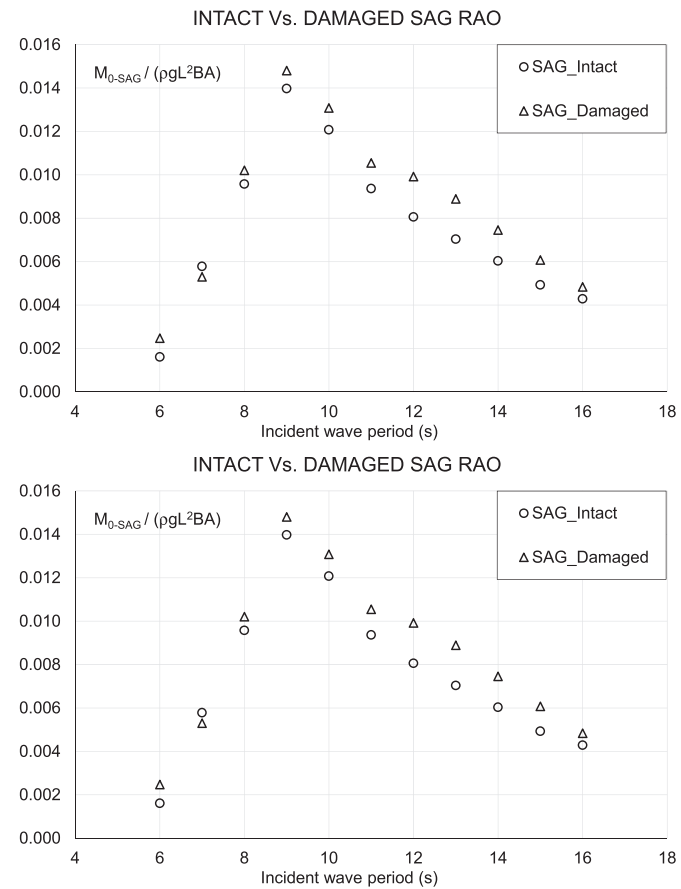


Fig. 22. Non-dimensional vertical bending moment Sagging- intact vs. damaged ship in head sea.

variation was carried out for the incident wave periods 9, 10, 11 and 12 s, corresponding to λ/λ_{OA} from 0.8 to 1.5. The range of measured H/λ_W variation is reported in Table 7 together with the corresponding wave height in ship scale. In beam seas, only a wave of 10 s period and intact ship has been considered. The range of variation was limited to smaller waves due to the very large amplitudes of roll motion observed (about 25 degrees). Therefore the H/λ_W was fixed at 1/45, 1/90 and 1/111, which corresponds to the wave heights of 3.36, 1.70 and 1.56 m respectively.

The results for head seas for the intact and damaged ships are shown in Figs. 29–35. In Figs. 29 and 30 the examples of time histories are given for the vertical shear force and for the vertical bending moment. The curves are relative to the test at $T=10$ s, i.e. $\lambda_W/\lambda_{OA}=1.02$;

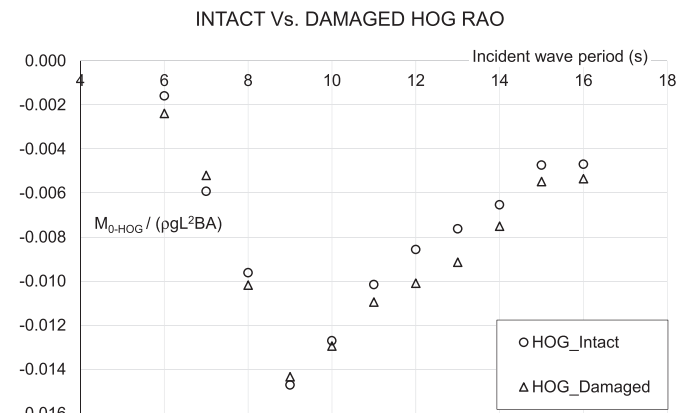


Fig. 23. Non-dimensional vertical bending moment Hogging- intact vs. damaged ship in head sea.

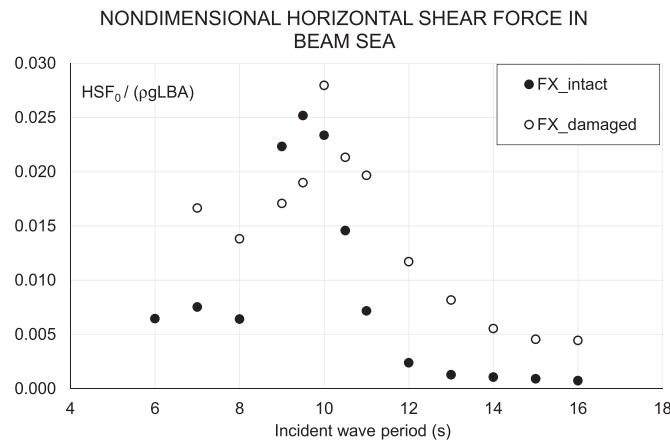


Fig. 24. Non-dimensional horizontal shear force intact vs. damaged ship in beam sea.

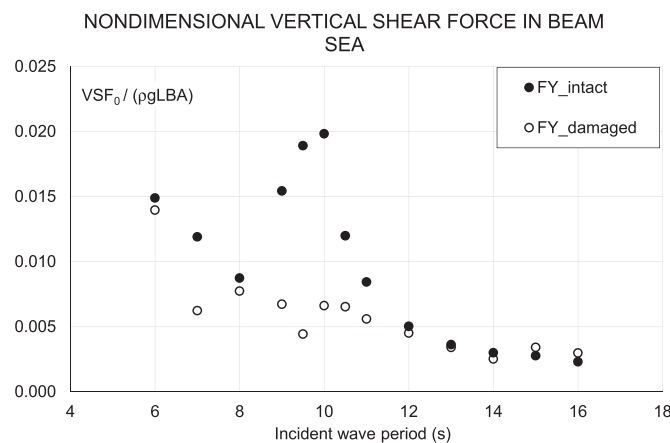


Fig. 25. Non-dimensional vertical shear force intact vs. damaged ship in beam sea.

only ten seconds of tests are presented to observe the changing of responses with the increasing of amplitude. For the same tests, the Fast Fourier Transform has been performed and one can observe the second-order harmonics in the VSF responses but not in the VBM responses. The head seas results are presented in a standard non-dimensional form as shown in Figs. 32–35, considering the same definition of force and moment amplitudes as defined in (10). It can be seen from Figs. 32 and 34, that the vertical shear forces for both the intact ship and the damaged ship have strong dependency on the wave amplitude for all four wave frequencies considered. The vertical bending moment values, reported in Figs. 33 and 35, show a nonlinear

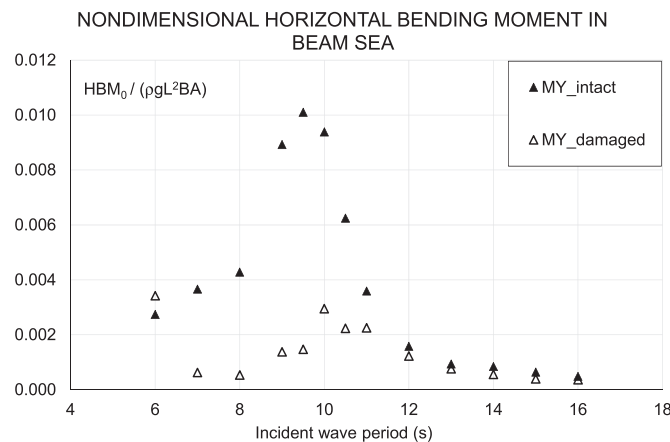


Fig. 26. Non-dimensional horizontal bending moment – intact vs. damaged ship.

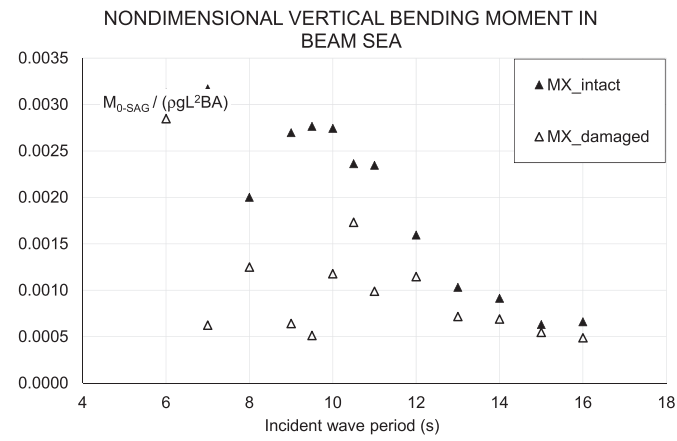


Fig. 27. Non-dimensional vertical bending moment - intact vs. damaged ship.

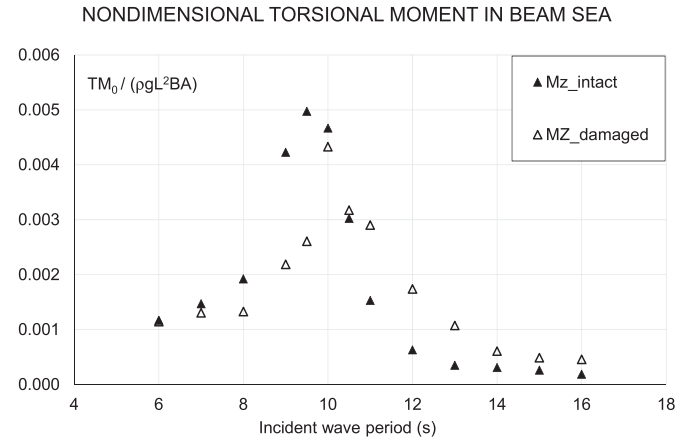


Fig. 28. Non-dimensional torsional moment - intact vs. damaged ship.

Table 6
Ratio between Loads in Damaged and Intact condition for head seas.

T_W (s)	VSF_D/VSF_I	SAG VBM_D/VBM_I	HOG VBM_D/VBM_I
6	0.729	1.536	1.502
7	1.159	0.916	0.878
8	1.303	1.066	1.058
9	1.269	1.059	0.975
10	1.318	1.083	1.019
11	1.415	1.126	1.078
12	1.860	1.231	1.179
13	1.996	1.263	1.199
14	2.003	1.236	1.148
15	2.059	1.232	1.157
16	1.635	1.129	1.140

Table 7
Summary of tests with amplitude variation.

T_W (s)	9	10	11	12
λ_W/L_{OA}	0.826	1.020	1.234	1.469
H/λ_W	1/40; 1/28; 1/22	1/40; 1/28; 1/22	1/40; 1/28; 1/22	1/40; 1/28; 1/22
H (m)	3.01; 4.55; 8.04	3.95; 5.36; 6.62	5.18; 7.15;	6.06; 8.20; 10.22

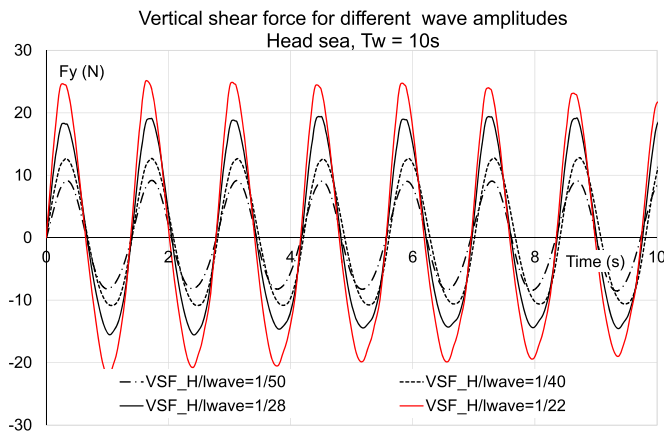


Fig. 29. Time history of shear force for different wave amplitudes for intact model in head sea, wave period=10 s.

behaviour at 9 s wave period while at the other three wave lengths the RAOs show almost linear behaviour as wave amplitudes vary; in fact it is in line with the absence of the second-order harmonics in Fig. 31 for the $\lambda_w/L_{OA}=1.02$. It can be highlighted that the vertical bending moment nonlinearities with respect to the wave amplitude variations are only present at certain wave frequencies, as concluded also by Korkut et al. (2005). The results for the intact ship in beam seas are shown in Figs. 36 and 37 for the HSF and the HBM responses. During these tests the wave amplitude was decreased due to the very high measured roll angles and a very strong variation of non-dimensional responses for the wave frequencies tested was observed.

6. Comparisons between the data obtained in this study and those obtained from Lee et al. (2012)

In Figs. 38–44, the comparison of the experimental results reported by Lee et al. (2012), Begovic et al. (2011) and the results of this study are given. It has to be highlighted that the data in Begovic et al. (2011) are obtained by testing the same model and using the same load cell as in Lee et al. (2012), but tested at in the towing/wave tank at the University of Strathclyde, while the results reported here were obtained using the same ship dimensions at a different scale. The damage scenario (two compartments damage) and inertial properties of the intact model in all campaigns were the same. In the following Table 8 a summary of results reported in the previous experimental campaigns is given.

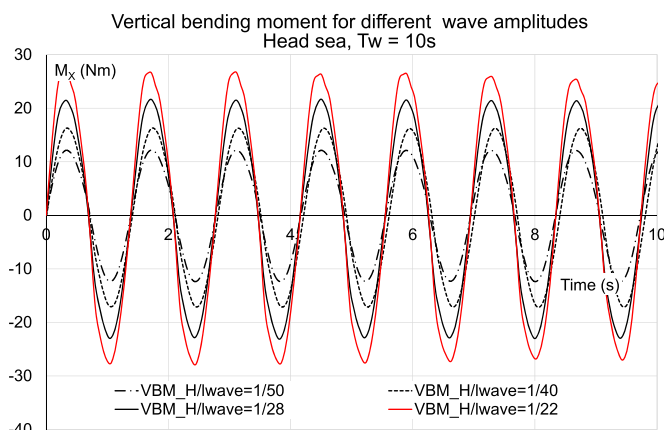


Fig. 30. Time history of shear force for different wave amplitudes for intact model in head sea, wave period=10 s.

The current study reports the results, especially for the intact ship, not reported in Lee et al. (2012), to give a complete set of hull girder load values. Furthermore, more tests in the range of wave periods from 8 to 13 s has been carried out to provide more data for a benchmarking of the results obtained from different numerical methods. For the comparison of the vertical bending moment, from different studies, the HOG and SAG amplitudes, given in Figs. 22 and 23 are summed up and the mean values are plotted against Lee et al. (2012) and Begovic et al. (2011) data, as shown in Figs. 39, 40 and 43.

The forces and moments presented in Begovic et al. (2011) have been reported in a non-dimensional form dividing by $0.5pgLB$ and $0.5pgL^2B$ respectively. To compare them with the current study they have been multiplied by 0.5.

From Fig. 38, very fair repeatability of results for the vertical shear forces for two intact geosim models in head seas, tested by the authors can be observed. In Fig. 39, the vertical bending moment values of the intact ship in head seas, obtained from three studies, are given. The differences between the small waves and large waves series from Lee et al. (2012), indicate that the measurements in the current study were carried out in “larger waves” than “large waves” and this is the principal source of difference among results from two experimental studies. The results from Begovic et al. (2011) further confirm this conclusion.

For the intact ship in the beam sea, Lee et al. (2012) reported the results of the VBM measurements only, although in this study higher responses were measured in the horizontal plane, i.e. HSF and HBM, as can be seen from Figs. 9–13. The VBM values for the beam seas, reported in Fig. 40, are significantly different in the two investigations, but since the magnitude of the loads are small this may not be of a major interest; whereas it will be of more interest to compare HBM values, where we would have expected low differences between the results. In Fig. 41 HBM values are compared for the current study and the results given in Begovic et al. (2011). It can be seen again that the variation of the wave amplitude in tests with the small model leads to the differences higher than between two studies.

Regarding the responses for the damaged ship, all available data in three studies are compared. In Fig. 42, vertical shear force RAOs results from Lee et al. (2012) and current study are compared and fair correlation except at the 10 s wave has been obtained. It can be noted that the 10 s wave is the only point where there is no difference between “Large Waves” and “Small Waves” series, what is rather strange, as this range is close to the resonance period and the nonlinearity with the wave amplitude variation is expected. The results from Begovic et al. (2011) at the wave periods from 8 to 11 s have significant differences from the current study. The difference at wave period 11 s is of the same order of magnitude as in the Lee and current study at 10 s wave. Therefore, the observed differences are attributed to the different wave steepness and the sensitivity of RAO results on wave amplitudes.

The torsional moment measurements are compared in Fig. 43, and it can be observed that in Lee et al. (2012) the missing wave periods of 11, 12 and 13 s are not making possible to obtain a complete correlation. In Fig. 44, the vertical bending moment values are compared and a fair correlation of results obtained from three studies can be noted.

The horizontal bending moment values for head sea from both campaigns has some irregularities, in Lee et al. (2012), an extremely high value at 14 s wave period occurs, while in the current study the value at 9 s wave period is higher than expected. The diagram with comparison of these experimental data has not been reported as the HBM values in head seas may not be of a major interest. For the same reason the VSF and VBM results for the damaged model in beam seas are not reported.

Regarding the torsion moment values of the damaged model in beam seas, given in Fig. 45 in Lee et al. (2012) study seem to have some errors occurred during the measurement or the analysis of the data since the values are almost zero in the whole wave frequency range. The

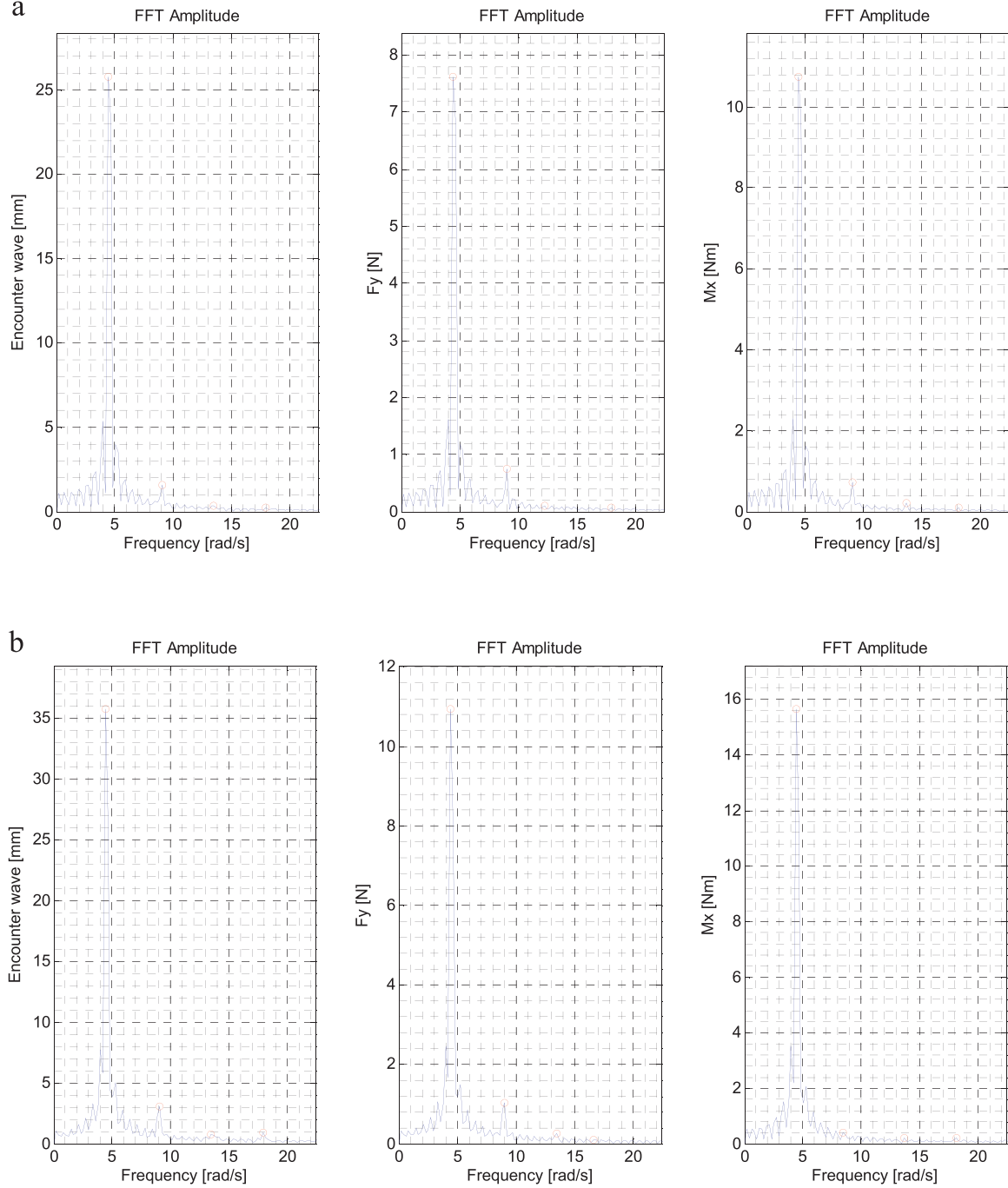


Fig. 31. a. FFT of wave, VSF and VBM for $H/\lambda_w=1/50$. b. FFT of wave, VSF and VBM for $H/\lambda_w=1/40$. c. FFT of wave, VSF and VBM for $H/\lambda_w=1/28$. d. FFT of wave, VSF and VBM for $H/\lambda_w=1/22$.

results from Begovic et al. (2011) and the current study indicate very good correlation of the measured data. The horizontal bending moment values, shown in Fig. 46, indicate that in the range of long waves the measured results obtained from three studies are very close. Regarding the data from Lee et al. (2012) it can be noted that there are some data missing which would have been very helpful for the correlations and there is a significant difference at the shortest wave. The results from Begovic et al. (2011) and the current study indicate very good correlation of the measured data.

Regarding the comparisons made in this study, it can be observed that the vertical bending moment and vertical shear force values in

head seas are generally in fair agreement between the three studies. Regarding the results in beam seas from the current study and Lee et al. (2012), the overall agreement of loads in vertical plane (VSF, VBM, TM) is poor. The comparisons of HSF and HBM values have not been possible for intact ship due to the missing data, and for the damaged ship, some missing data at certain frequencies reported in Lee et al. (2012) would have been very helpful. The results from Begovic et al. (2011) enable us to explain some experimental trends as they are relative to the same model as the one used in Lee et al. (2012) and are tested by the authors of the current study.

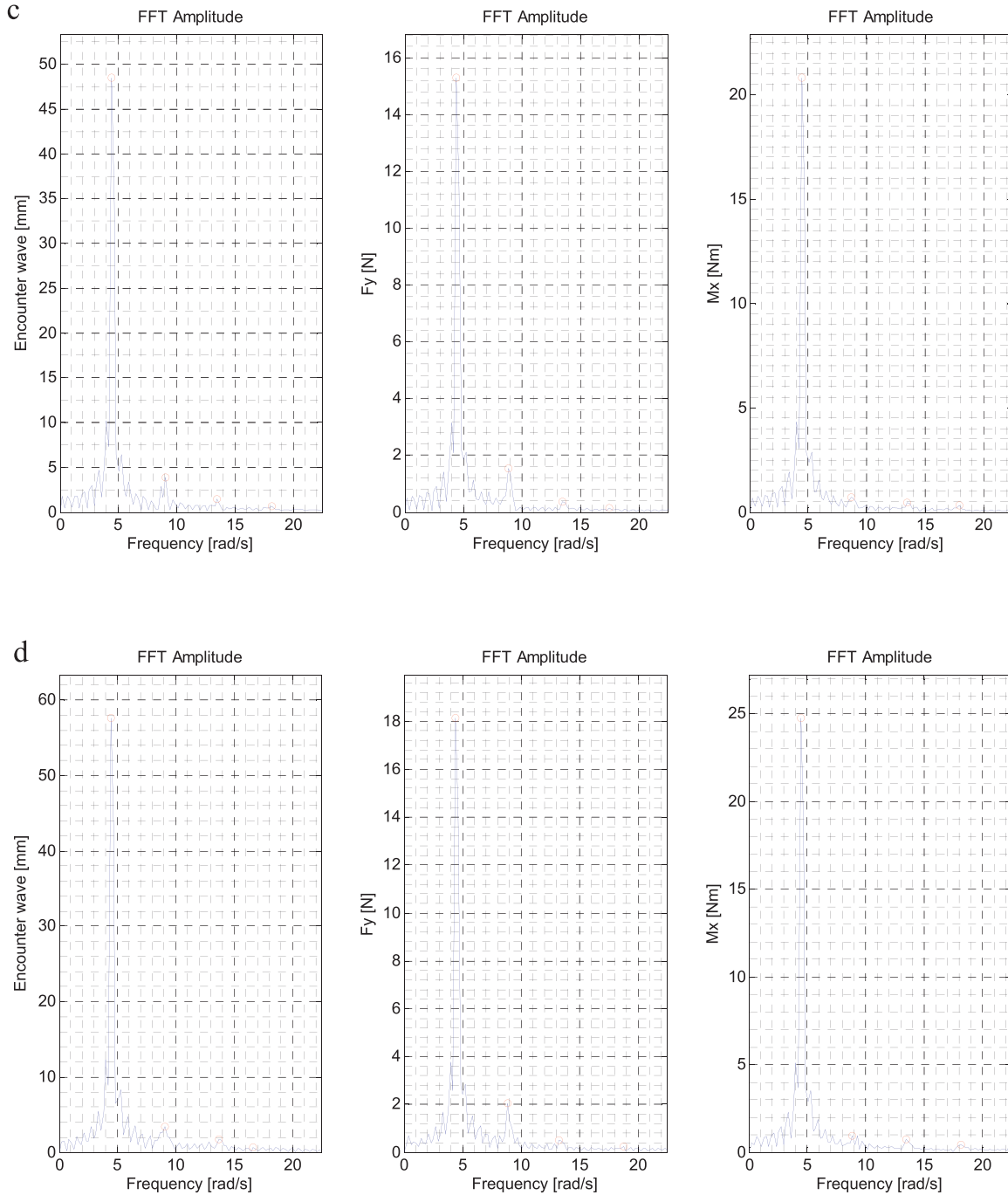


Fig. 31. (continued)

7. Conclusions

The main aim of this study was to provide a benchmark data on global loads acting on intact and damaged DTMB 5415 navy vessel in regular waves at zero speed. The experimental campaign presented here is the continuation of the previous work by Begovic et al., (2011, 2013) dealing with the ship motions in the same conditions.

The results show that the two compartment symmetric damage located abaft midship significantly increases the roll damping of the ship due to the waves and vortices generation during movement of flood water inside and outside of the compartment. This additional roll damping has been analysed in terms of equivalent damping, based on

the experimental time histories of the roll motion in a free oscillation test reporting the linear and quadratic roll extinction coefficients and the roll periods of intact and damaged model. For the damage scenario considered, both the linear and quadratic extinction coefficients have been doubled compared to the intact case.

The results for the vessel motions show that repeatability with the previous experimental campaign is generally good although some unexplained discrepancies occur at 11 s wave period. As regard to the uncertainty of the experiments carried out, almost all responses are in the range up to 3%. A comparison of results in beam seas between a soft-moored vessel and a freely drifting vessel show that the motions are very similar especially in the long waves. The differences in the hull

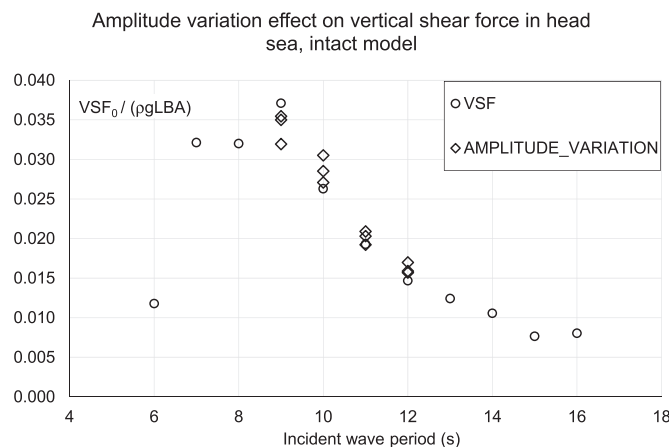


Fig. 32. Nonlinearities in vertical shear force head sea, intact model.

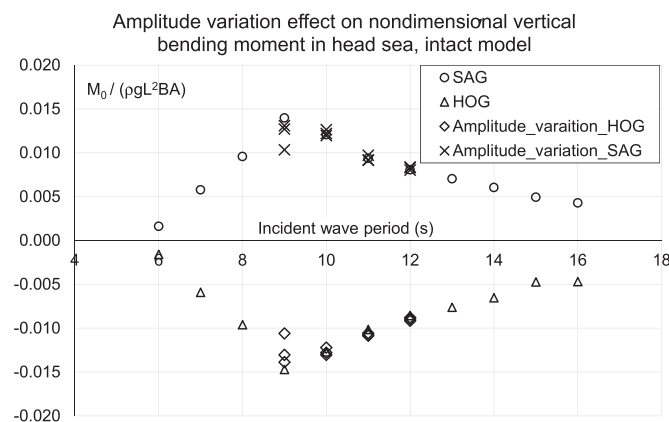


Fig. 33. Nonlinearities in bending moment, head sea, intact model.

girder loads are up to 10% but the shifting of resonant frequency suggested the choice a free drifting model setup is the most appropriate.

Regarding the measured loads, the structural response values of the damaged model are greater than those on the intact model for most of the modes of motion with the exception of the vertical and horizontal bending moments in the beam seas condition. The ratio of the damaged and intact vertical bending moment values at each tested wave frequency is calculated and discussed with respect to the results reported in the literature. It can be noted that there is a high discrepancy in the results as reported by different authors, ranging

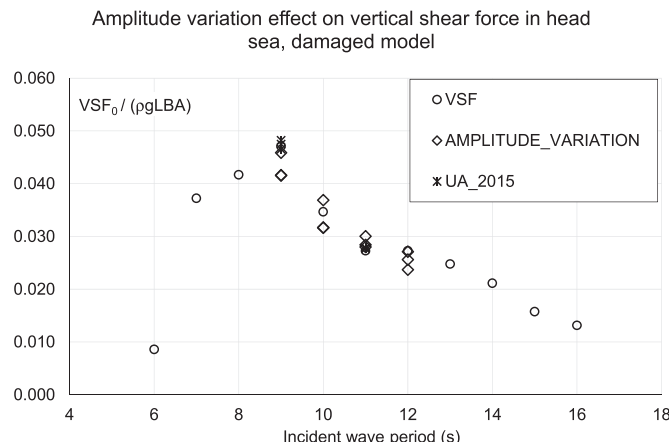


Fig. 34. Nonlinearities in vertical shear force, head sea, damaged model.

from 1.10 up to 2 and the future work should investigate this issue further.

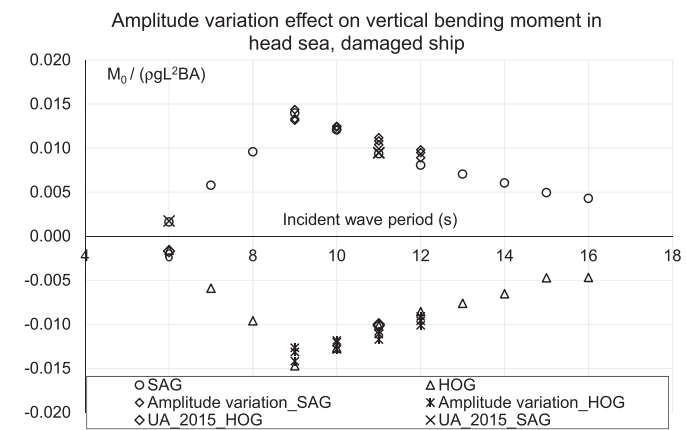


Fig. 35. Nonlinearities in vertical bending moment, head sea, damaged model.

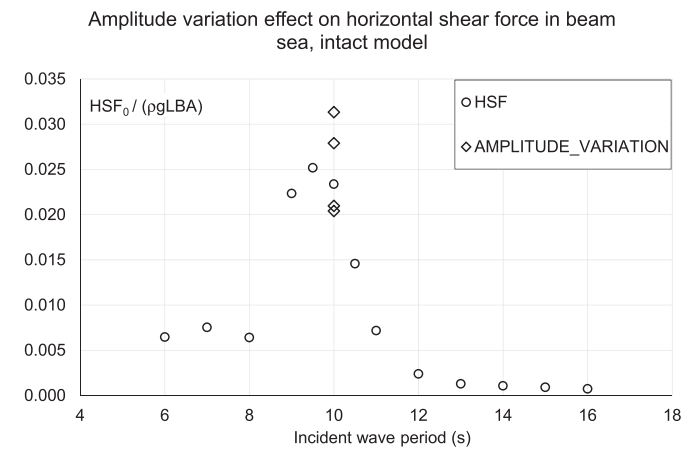


Fig. 36. Nonlinearities in horizontal shear force beam sea, intact model, free drift.

In this work a particular attention was focused on the nonlinearities in global loads as the wave amplitudes vary. In general, it can be highlighted that the vertical shear force and the vertical bending moment values both for the intact and damaged ships exhibit a strong dependency on wave amplitude variations at the wave frequencies around the natural frequencies of the vessel. It can be further noted that the vertical shear force values have appreciable second-order harmonics in a range of frequencies when the wave amplitudes varied for λ/L from 0.8 to 1.5.

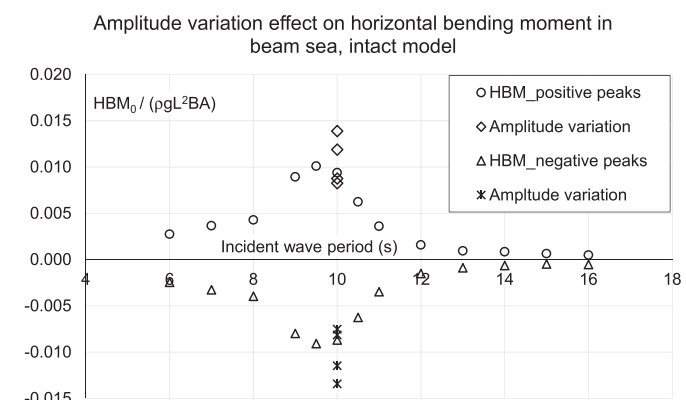


Fig. 37. Nonlinearities in horizontal bending moment, beam sea, intact model, free drift.

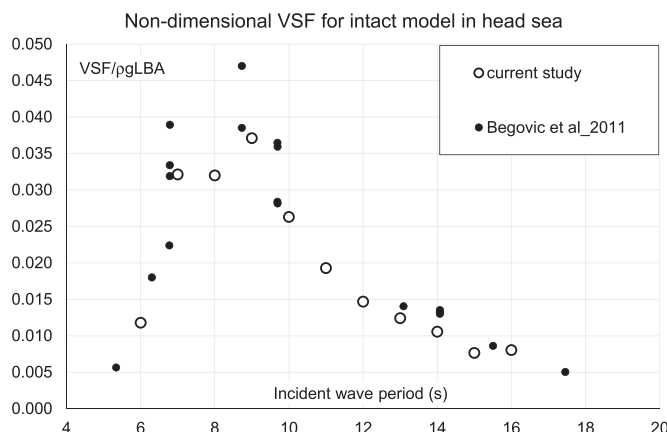


Fig. 38. Benchmarking of vertical shear force in head seas – intact model (Fig. 9 from Begovic et al. (2011)).

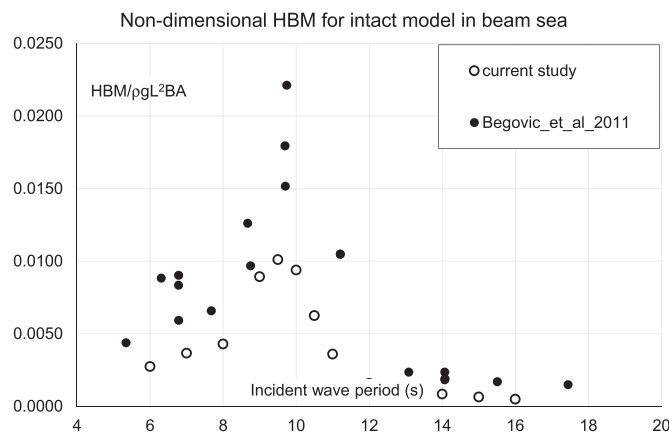


Fig. 41. Benchmarking of horizontal bending moment in beam seas – intact model (Fig. 14 from Begovic et al. (2011)).

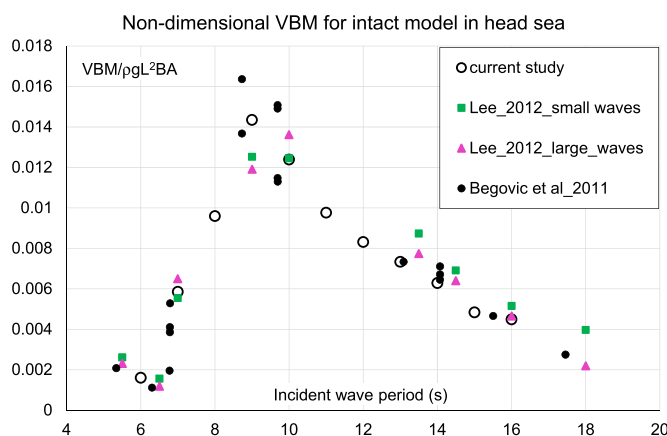


Fig. 39. Benchmarking of vertical bending moment in head seas – intact model (Fig. 22 from Lee et al. (2012) and Fig. 10 from Begovic et al. (2011)).

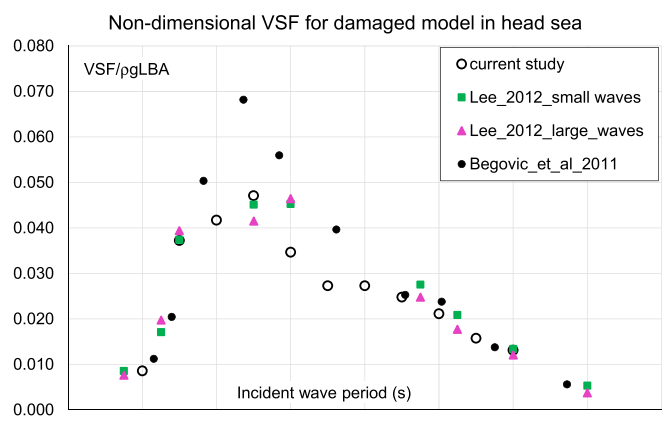


Fig. 42. Benchmarking of vertical shear force in head seas – damaged model (Fig. 25 from Lee et al. (2012), Fig. 17 from Begovic et al. (2011)).

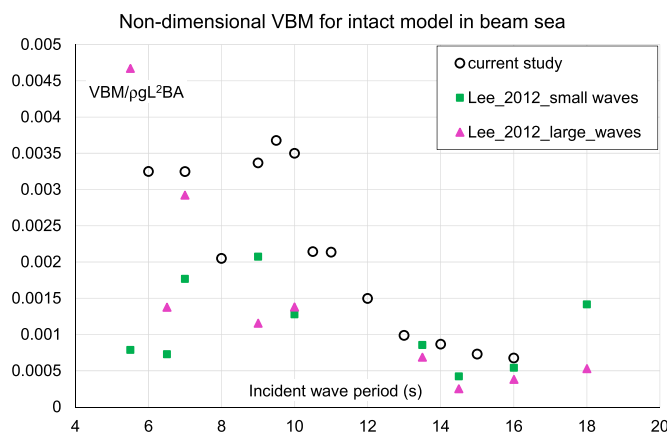


Fig. 40. Benchmarking of vertical bending moment in beam seas – intact model (Fig. 24 from Lee et al. (2012)).

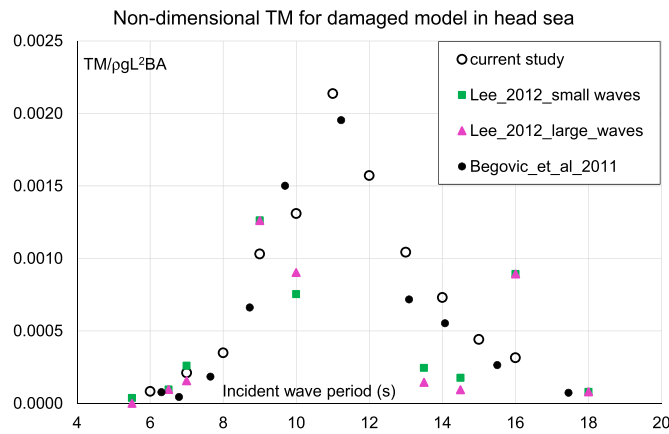


Fig. 43. Benchmarking of torsional moment in head seas – damaged model (Fig. 26 from Lee et al. (2012)).

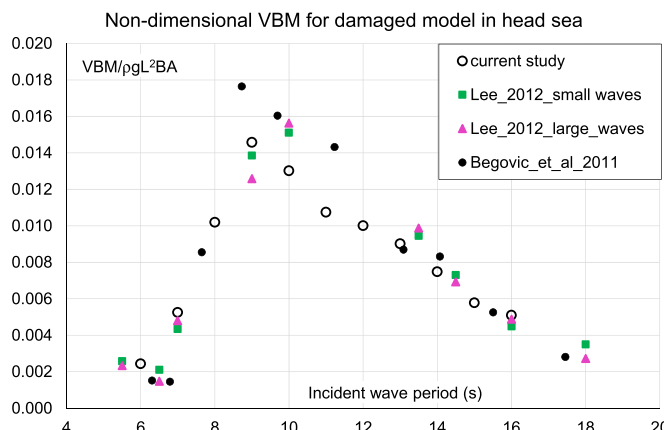


Fig. 44. Benchmarking of vertical bending moment in head seas – damaged model (Fig. 27 from Lee et al. (2012), Fig. 18 from Begovic et al. (2011)).

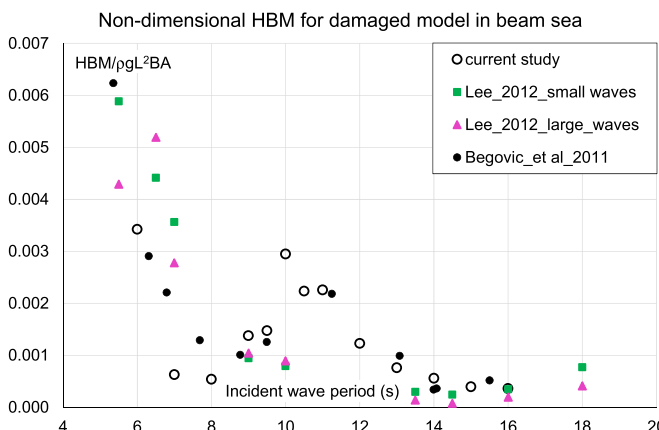


Fig. 46. Benchmarking of horizontal bending moment in beam seas – damaged model (Fig. 36 from Lee et al. (2012)).

Table 8

Summary of experimental study carried out by Lee et al. (2012) and Begovic et al. (2011).

Considered Load	SHIP condition	Heading	Fig. No Lee et al. (2012)	Fig. No Begovic et al. (2011)	Current study	Benchmark
VSF	Intact	Head sea	Not given	9	21	38
VBM	Intact	Head sea	22	10	22, 23	39
HSF	Intact	Beam sea	Not given	12	24	–
TM	Intact	Beam sea	Not given	13	28	–
VBM	Intact	Beam sea	24	Not given	12	40
HBM	Intact	Beam sea	Not given	14	11	41
VSF	Damaged	Head sea	25	17	21	42
TM	Damaged	Head sea	26	Not given	43	43
VBM	Damaged	Head sea	27	18	22, 23	44
HBM	Damaged	Head sea	28	Not given	44	Not given
VSF	Damaged	Beam sea	33	Not given	25	Not given
HSF	Damaged	Beam sea	Not given	20	24	–
TM	Damaged	Beam sea	34	21	28	45
VBM	Damaged	Beam sea	35	Not given	27	Not given
HBM	Damaged	Beam sea	36	22	26	46

Finally, the results obtained for loads measurements have been compared against Lee et al. (2012) and Begovic et al. (2011), trying to provide more complete set of data for the intact and damaged ship. Regarding the comparison made in this study, it can be observed that the vertical bending moment and vertical shear force values in head seas, as well as horizontal shear force and horizontal bending moment in beam seas are generally in fair agreement between the three studies in beam seas are generally in fair agreement between the three studies

and often the wave amplitude variation is the principal source of difference among results.

Acknowledgements

The Authors gratefully acknowledge the help and contributions made by Mr. Charles. Keay and Mr. Edd Nixon, technical staff of the Kelvin Hydrodynamics Laboratory, Strathclyde University, Glasgow, during the preparation and performance of the experimental campaign reported in this paper.

References

- Begovic, E., Mortola, G., Incecik, A., Day, A.H., 2013. Experimental assessment of intact and damaged ship motions in head, beam and quartering seas. *Ocean Eng.* 72 (2013), 209–226. <http://dx.doi.org/10.1016/j.oceaneng.2013.06.024>.
- Begovic, E., Incecik, A., Day, A.H., 2011. Experimental assessment of intact and damaged ship motions in head, beam and quartering seas. In: HSMV Conference 2011, Naples, Italy.
- Bulian, G., Francescutto, A., Fucile, F., November 2009. Determination of Relevant Parameters for the Alternative Assessment of Intact Stability Weather Criterion On Experimental Basis, Project HYD-III-CEH-5, Rev.1.0-Final-22. Available at (www.shipstab.org)
- Buzanicic-Primorac, B., Corak, M., Parunov, J., 2015. Statistics of still water bending moment of damaged ship. In: Guedes, Soares, Shenoi (Eds.), *Analysis and Design of Marine Structures*. Taylor & Francis Group, London, 491–497.
- Chakrabarti, S.K., 1994. Offshore structure modelling. In: *Advances Series in Ocean Engineering*, Worlds Scientific Publishing Co. vol. 9, Feb.
- Day, A.H., Clelland, D., Valentine, G., 2011. Development of a low cost laser wave measurement system, In: Proceedings of the Second International Conference on Advanced Model Measurement Technology (AMT'11), Newcastle, April.

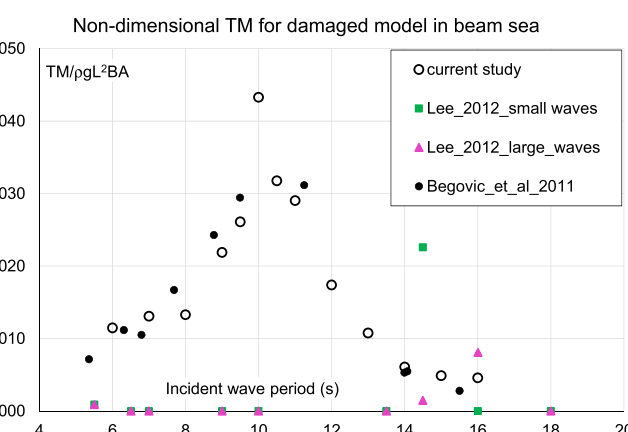


Fig. 45. Benchmarking of torsional bending moment in beam seas – damaged model (Fig. 34 from Lee et al. (2012), Fig. 21 from Begovic et al. (2011)).

- Domeh, V.D.K., Sobey, A.J., Hudson, D.A., 2015. A preliminary experimental investigation into the influence of compartment permeability on damaged ship response in waves. *Appl. Ocean Res.* 52 (2015), 27–36. <http://dx.doi.org/10.1016/j.apor.2015.05.001>.
- Fonseca, N., Guades Soares, C., 2002. Comparison of numerical and experimental results of nonlinear wave-induced ship motions and loads. *J. Mar. Sci. Technol.* 2002 (6), 193–204.
- Fonseca, N., Guades Soares, C., 2004a. Experimental investigation of the nonlinear effects on the vertical motions and loads of a containership in regular waves. *J. Ship Res.* 48 (2), 118–147.
- Fonseca, N., Guades Soares, C., 2004b. Experimental investigation of the nonlinear effects on the statistics of vertical motions and loads of a containership in irregular waves. *J. Ship Res.* 48 (2), 148–167.
- Hirdaris, S.E., Bai, W., Dessi, D., Ergin, A., Gu, X., Hermundstad, O.A., Huijsmans, R., Iijima, K., Nielsen, U.D., Parunov, J., Fonseca, N., Papanikolaou, A., Argyriadis, K., Incecik, A., 2014. Loads for use in the design of ships and offshore structures. *Ocean Eng.* 78 (2014), 131–174. <http://dx.doi.org/10.1016/j.oceaneng.2013.09.012>.
- ITTC – Recommended Procedures and Guidelines, 2011. Numerical Estimation of Roll Damping. 7.5-02-07-04.5.
- Korkut, E., Atlar, M., Incecik, A., 2004. An experimental study of motion behavior with an intact and damaged Ro-Ro ship model. *Ocean Eng.* 31 (2004), 483–512.
- Korkut, E., Atlar, M., Incecik, A., 2005. An experimental study of global loads acting on an intact and damaged Ro-Ro ship model. *Ocean Eng.* 32 (2005), 1370–1403.
- Kukkanen, T., Matusiak, J., 2014. Non linear hull girder loads of a RoPax ship. *Ocean Eng.* 75 (2014), 1–14. <http://dx.doi.org/10.1016/j.oceaneng.2013.10.008>.
- Lee, Y., Chan, H.S., Pu, Y., Incecik, A., Dow, R.S., 2012. Global wave loads on a damaged ship. *Ships Offshore Struct.* 7 (3), 237–268. <http://dx.doi.org/10.1080/17445302.2011.588081>.
- Manderbacka, T., Ruponen, P., Kulovesi, J., Matusiak, J., 2015. Model experiments of the transient response to flooding of the box shaped barge. *J. Fluid Struct.* 57 (2015), 127–143. <http://dx.doi.org/10.1016/j.jfluidstructs.2015.06.002>.
- O'Dea J. Powers E., Zselecsky J., 1992. Experimental determination of non-linearities in vertical plane ship motions. In: Proceedings of the 19th Symposium on Naval Hydrodynamics, Seoul, Korea, pp. 73–91
- Parunov, J., Corak, M., Gledic, I., 2015. Comparison of two practical methods for seakeeping assessment of damaged ships. In: Guedes, Soares, Shenoi (Eds.), *Analysis and Design of Marine Structure*. Taylor & Francis Group, London, 37–44.
- Song, M.J., Kim, K.H., Kim, Y., 2011. Numerical analysis and validation of weakly nonlinear ship motions and structural loads on a modern containership. *Ocean Eng.* 38 (2011), 77–87. <http://dx.doi.org/10.1016/j.oceaneng.2010.09017>.
- Watanabe, I., Keno, M., Sawada, H., 1989. Effect of bow flare on shape to wave loads of a container ship. *J. Soc. Nav. Archit. Jpn.* 1989 (166), 259–266.
- Zhu, S., Moan, T., 2013. New insight into the wave-induced nonlinear vertical load effects of ultra-large container ships based on experiments. *J. Mar. Sci. Tecnol.* 18 (2013), 87–114. <http://dx.doi.org/10.1007/s00773-012-0186-x>.
- Zhu, S., Moan, T., 2014. Nonlinear effects from wave-induced maximum vertical bending moment on a flexible ultra-large containership model in severe head and oblique seas. *Mar. Struct.* 35, 1–25.